Fluid-induced breakdown of white mica controls nitrogen transfer during fluid-rock interaction in subduction zones

Ralf Halama[1,*], Gray E. Bebout[2], Horst R. Marschall[3,4], Timm John[5]

[1] School of Geography, Geology and the Environment, Keele University, Keele, ST5 5BG, United Kingdom

[2] Department of Earth and Environmental Sciences, Lehigh University, 1 West Packer Avenue, Bethlehem, Pennsylvania 18015, USA

[3] Department of Geology and Geophysics, Woods Hole Oceanographic Institution, 266 Woods Hole Rd., Woods Hole, Massachusetts 02543, USA

[4] Goethe-Universität Frankfurt, Institut für Geowissenschaften, Altenhöferallee 1, 60348 Frankfurt am Main, Germany

[5] Institut für Geologische Wissenschaften, Freie Universität Berlin, Malteserstr. 74-100, 12249 Berlin, Germany

* Corresponding author contact information:
Ralf Halama
School of Geography, Geology and the Environment
Keele University, Keele, ST5 5BG, United Kingdom
E-mail: r.halama@keele.ac.uk
Tel: +44-1782-734960

Word count: 6310

Revised version, submitted to **International Geology Review** ***09/2016***

Abstract

In order to determine the effects of fluid-rock interaction on nitrogen elemental and isotopic systematics in high-pressure metamorphic rocks, we investigated three different profiles representing three distinct scenarios of metasomatic overprinting. A profile from the Chinese Tianshan (ultra)high pressure – low temperature metamorphic belt represents a prograde, fluid-induced blueschist-eclogite transformation. This profile shows a systematic decrease in N concentrations from the host blueschist (~26 µg/g) via a blueschist-eclogite transition zone (19-23 µg/g) and an eclogitic selvage (12-16 µg/g) towards the former fluid pathway. Eclogites and blueschists show only a small variation in $\delta^{15}N_{air}$ (+2.1±0.3‰), but the systematic trend with distance is consistent with a batch devolatilization process. A second profile from the Tianshan represents a retrograde eclogite-blueschist transition. It shows increasing, but more scattered N concentrations from the eclogite towards the blueschist and an unsystematic variation in $\delta^{15}N$ values ($\delta^{15}N$ = +1.0 to +5.4‰). A third profile from the high-*P/T* metamorphic basement complex of the Southern Armorican Massif (Vendée, France) comprises a sequence from an eclogite lens via retrogressed eclogite and amphibolite into metasedimentary country rock gneisses. Metasedimentary gneisses have high N contents (14-52 µg/g) and positive $\delta^{15}N$ values (+2.9 to +5.8‰), and N concentrations become lower away from the contact with 11-24 µg/g for the amphibolites, 10-14 µg/g for the retrogressed eclogite, and 2.1-3.6 µg/g for the pristine eclogite, which also has the lightest N isotopic compositions ($\delta^{15}N$ = +2.1 to +3.6‰).

Overall, geochemical correlations demonstrate that phengitic white mica is the major host of N in metamorphosed mafic rocks. During fluid-induced metamorphic overprint, both abundances and isotopic composition of N are controlled by the stability and presence of white mica. Phengite breakdown in high-*P/T* metamorphic rocks can liberate significant amounts of N into the fluid. Due to the sensitivity of the N isotope system to a sedimentary signature, it can be used to trace the extent of N transport during metasomatic processes. The Vendée profile demonstrates that this process occurs over several tens of meters and affects both N concentrations and N isotopic compositions.

Keywords:

Nitrogen, N isotopes, white mica, fluid-rock interaction, subduction, high-pressure metamorphic rocks

1. Introduction

Understanding the processes that affect both elemental concentrations as well as isotopic signatures in subducting rocks are of fundamental importance for the assessment of subduction zone cycling of elements (e.g., Bebout 2007, 2014; Marschall *et al.* 2007a; Halama *et al.* 2011; John *et al.* 2004, 2011; Spandler and Pirard 2013; Konrad-Schmolke and Halama 2014; Bebout and Penniston-Dorland 2016). Elemental and isotopic fractionation during subduction-zone metamorphism and metasomatism influences the balance of input and output in subduction zones and the geochemical signatures transported into the deep mantle beyond the arc, potentially resurfacing via plume-related magmatism. Metamorphic rock sequences that record the successive advance of a metamorphic/metasomatic process provide a valuable means to evaluate the magnitude and extent of geochemical effects via fluid-rock interaction during subduction cycling.

The nitrogen (N) isotope system has a great potential as geochemical tracer for crustal and volatile recycling due to the large isotopic differences in the various terrestrial reservoirs (Busigny and Bebout 2013; Halama *et al.* 2014; Johnson and Goldblatt 2015; Bebout *et al.* 2016; Mikhail and Howell 2016). Nitrogen is a sensitive tracer for fluid-rock interaction and metasomatic processes (Bebout 1997; Halama *et al.* 2010; Li *et al.* 2014), in particular for sediment-derived fluids because N is largely fixed by organic processes in sedimentary environments (Bebout 1997; Bebout *et al.* 2016). However, direct evidence of spatially constrained transport of N is rare, and the processes that cause N mobilization and fractionation of N isotopes need to be better understood. It has been established for some metasedimentary suites that N contents decrease and $\delta^{15}N$ values increase with increasing metamorphic grade during subduction (Bebout and Fogel 1992; Mingram and Bräuer 2001). However, other suites show relatively little change and N appears to be retained to depths approaching those beneath arcs (Busigny *et al.* 2003; Pitcairn *et al.* 2005). Similarly, metamorphosed mafic and ultramafic rocks appear to largely retain N to depths of at least 60-70 km (Halama *et al.* 2010, 2012; Busigny *et al.* 2011).

In this study, we use spatially constrained profiles of metamorphosed mafic igneous rocks that represent the frozen-in advance of fluid-induced metamorphic/metasomatic processes to investigate the behaviour of N and N isotopes during prograde and retrograde metamorphic changes. Three profiles were selected that represent i) a prograde transformation of blueschist into eclogite due to fluid ingress from a major fluid conduit (Beinlich *et al.* 2010; John *et al.* 2012), ii) a retrograde transformation of eclogite into blueschist during exhumation within a subduction channel (van der Straaten *et al.* 2012), and iii) an exhumation-related interaction of an eclogite body with surrounding felsic gneisses in a collisional context. The first two sample sequences come from the

south-eastern Tianshan (China) high-pressure low-temperature (HP-LT) belt, whereas the third profile is from the Variscan Belt in the Vendée (France). We find that prograde dehydration can release large amounts of N due to the breakdown of white mica, in which N is incorporated as ammonium (NH_4^+), whereas the associated isotopic changes are relatively small (< 1‰). Hence, non-altered eclogites should largely reflect the N isotopic composition of their protoliths. In contrast, interaction with retrograde fluids can impart the N elemental and isotopic characteristics of the rocks with which the fluid equilibrated and hence cause significant perturbations of the N systematics.

2. Geologic setting and sample description

2.1. Tianshan orogen, (ultra)high-pressure low-temperature ((U)HP-LT) metamorphic belt, China

Two profiles were sampled in a (U)HP-LT belt of metamorphic rocks in the Chinese part of the Tianshan orogen (Figure 1a). The Tianshan orogen extends morphologically over 2500 km from north-western China in the east over Kyrgyzstan and Kazakhstan to Tajikistan and Uzbekistan in the west along the southwestern margin of the Central Asian Orogenic Belt, also known as the Altaid Tectonic Collage (e.g., Şengör *et al.* 1993). In China, the western Tianshan, which includes the (U)HP metamorphic terrane, is situated between the Junggar plate in the north and the Tarim plate in the south (Gao *et al.* 2009 and references therein). The HP-LT rocks are interpreted as relics of the Palaeozoic South Tianshan Ocean basin and whole rock geochemical data of the mafic rocks show oceanic basalt affinities including former seamounts and young arcs, subducted during Silurian and Carboniferous time (Windley *et al.* 1990; Şengör and Natal'in 1996; Gao *et al.* 1998; Gao and Klemd 2003; John *et al.* 2008). The (U)HP–LT metamorphic terrane comprises predominantly metasediments, which form the host rocks of mafic metavolcanic rocks, metavolcaniclastics, marbles, and ultramafic rocks, and is considered to represent a tectonic mélange formed within an accretionary wedge-like setting on the southern margin of the Central Tianshan Arc terrane during the subduction of the South Tianshan Ocean (e.g., Gao *et al.* 1999; van der Straaten *et al.* 2008; Klemd *et al.* 2011). The mafic metavolcanic rocks (mainly eclogites locally interlayered with blueschists) occur irregularly distributed as differently sized pods, boudins, thin layers or large massive blocks embedded in voluminous metasedimentary host rocks or less abundant surrounded by metavolcaniclastic rocks (Gao and Klemd 2003). Blueschist occurrences

include prograde and retrograde varieties (Gao and Klemd 2001; Gao *et al.* 2007; van der Straaten *et al.* 2008, 2012; Beinlich *et al.* 2010). Peak-metamorphic conditions of most eclogites and prograde blueschists are similar (both lithologies occur locally with gradual transitions or intimately intercalated) and range between 480 and 580 °C at 1.4–2.3 GPa at a regional scale (e.g., Klemd *et al.* 2002; John *et al.* 2008). Moreover, relics of UHP conditions (e.g. coesite inclusions in garnet) or thermodynamic modelling suggesting UHP conditions for both metasediments and eclogites have been reported with peak P–T conditions of 570–630 °C at 2.7–3.3 GPa for eclogite-facies mica schists and 470–510 °C at 2.4–2.7 GPa for eclogites from several localities (Lü *et al.* 2008, 2009; Wei *et al.* 2009; Tian and Wei 2013). The juxtaposition of UHP and HP eclogite-facies rocks juxtaposed on a meter scale is thought to reflect mixing of eclogite-facies rock from different depths at the plate interface in a subduction channel-like setting (van der Straaten *et al.* 2008; Lü *et al.* 2009; Klemd *et al.* 2011). The timing of peak metamorphic conditions was determined by garnet growth ages of ca. 315 Ma based on multi-point Lu-Hf isochron ages for both blueschists and eclogites from various locations within the (U)HP-LT belt (Klemd *et al.* 2011). High-pressure veins crosscutting a blueschist wall-rock formed contemporaneously at 317 ± 5 Ma (Rb-Sr) which is consistent with metamorphic fluid release due to prograde transformations of blueschists to eclogites (John *et al.* 2012). U-Pb SIMS ages of metamorphic zircon rims in eclogites are indistinguishable within error at 319 ± 3 Ma (Su *et al.* 2010). The post-peak cooling was dated by white mica geochronology (K-Ar, Ar-Ar, Rb-Sr) and gave ages between 310 and 311 Ma (Klemd *et al.* 2005).

For the profiles, drill cores with a diameter of 2.54 cm and a length of about 10-15 cm were taken to obtain a good spatial resolution. At both sample localities, the samples occur as loose, meter-sized blocks, which have fallen from the steep mountain slopes as rock falls. The blocks represent a mixture of various rock types that are now found within and partly covered by quaternary deposits.

Profile 1 (JTS sequence; Figure 2a) represents the prograde transformation of blueschist into eclogite due to fluid infiltration. The JTS sequence was studied in detail by Beinlich *et al.* (2010) and John *et al.* (2012), and the following summary is based on these works. The massive blueschist with the main mineral assemblage garnet + glaucophane + omphacite + phengite + quartz is cross-cut by a carbonate-quartz vein, which is surrounded by an eclogitic reaction halo mainly composed of omphacite and garnet. The vein represents a major former fluid pathway that shows fluid infiltration from an external source and dehydration of the immediate wall rock. Important petrographic observations of the fluid-induced eclogitization include replacement of sodic amphibole by omphacitic clinopyroxene, increase in the modal abundances of quartz and carbonate

and decrease in the modal abundance of white mica with decreasing distance to the vein. The successive breakdown of white mica towards the vein is responsible for a relative depletion in large-ion lithophile elements (LILE: K, Rb, and Cs) in the eclogitic selvage compared to the host blueschist. Enrichments in Ca, Pb and Sr and depletions in HFSE can also be attributed to the fluid-induced eclogitization.

Profile 2 (FTS 9-1 sequence; Figure 2b) represents a gradual retrograde transition from eclogite to blueschist caused by fluid-rock interaction during uplift in the subduction channel (van der Straaten *et al.* 2008, 2012). The following description is based on the petrologic-geochemical investigation by van der Straaten *et al.* (2012) on these samples. The eclogitic parts consist of a fine-grained omphacite matrix with accessory rutile and porphyroblasts of garnet. The fluid-induced blueschist-facies overprint caused replacement of the eclogite-facies assemblage by newly formed glaucophane, paragonite, chlorite, calcite and titanite. The increase in the modal amounts of glaucophane, white mica and calcite with increasing blueschist-facies overprint lead to a nearly complete replacement of omphacite in the glaucophane schist.

2.2. Les Essarts Unit, Variscan Belt, Vendée, France

Samples were taken along a ~100 m long profile from an approximately 1 km thick eclogite lens via retrogressed eclogite and amphibolite into surrounding metasedimentary gneiss in the quarry "La Gerbaudière" of the Les Essarts Unit, 25 km south of Nantes and west of St. Philbert de Bouaine (Figure 1b). This unit constitutes a HP metamorphic basement complex of the Southern Armorican Massif that is part of the Variscan belt (Matte 2001). Rocks of oceanic origin (eclogites, amphibolites derived from eclogite, meta-plagiogranites and serpentinites) form several km-long stretched and slightly boudinaged lenses surrounded by foliated ortho- and paragneisses that are rich in white mica (Mauler *et al.* 2001). The eclogites have gabbroic protoliths with a crystallization age of 1297±60 Ma based on a zircon U-Pb upper intercept age (Peucat *et al.* 1982). The eclogite-facies metamorphism was dated at 436±15 Ma based on a zircon U-Pb lower intercept age (Peucat *et al.* 1982). The primary HP mineral assemblage is omphacite + garnet + rutile ± quartz ± kyanite ± zoisite ± magnesio-hornblende ± pyrite ± chalcopyrite and peak P-T conditions are 1.6-2.0 GPa and 650-750 °C (Godard 2009). A major deformation event occurred during the eclogite-facies metamorphism, followed by retrogression that transformed most of the eclogites into amphibolites, in particular affecting the margins of the eclogite lenses. Retrogression is indicated by presence of green amphibole and plagioclase-clinopyroxene symplectite along omphacite grain boundaries

(Mauler *et al.* 2001). The gneisses surrounding the eclogites with the main mineral assemblage quartz + plagioclase + biotite + garnet + white mica are of continental origin and record two distinct episodes of high-grade metamorphism (Godard 2009). The first event comprises intrusion of granite and migmatisation of cordierite-bearing metapelites (T ~ 670°C, P = 0.3 GPa) within the pre-Variscan continental crust. The second event is an eclogite-facies overprint, cofacial with the eclogitization of the adjacent oceanic mafic rocks at peak P-T conditions of P > 1.6 GPa and T ~ 700°C, which occurred during eo-Variscan subduction (Bernard-Griffiths and Cornichet 1985; Godard 2009) with simultaneous deformation of eclogites and gneisses. Several coronitic and pseudomorphic reactions caused the growth of high-pressure minerals (garnet, kyanite, phengite, rutile) and the expense of the previous high-temperature parageneses (Godard 2009). The Les Essarts Unit is interpreted as tectonic mélange of pre-Variscan oceanic and continental crusts that were eclogitized during subduction and subsequently incorporated into the Variscan orogenic belt (Godard 2001).

[Figure 1 near here]
[Figure 2 near here]

3. Analytical methods

3.1. Nitrogen content and nitrogen isotopic compositions

Nitrogen concentrations and isotopic compositions of bulk rock powders were analysed at Lehigh University. Sample preparation and analytical protocol follow the methods described in Bebout *et al.* (2007). In brief, about 100-250 mg of sample powder and Cu/CuOx reagent are evacuated for 24 h before sealing, with intermittent heating to ~ 100 °C. Nitrogen is extracted at 1000 °C and transferred as N_2 into a Finnigan MAT 252 mass spectrometer using a Finnigan Gas Bench II and a U-trap interface in which samples of N_2 are entrained in a He stream. Details regarding the calculation of N concentrations in unknowns and reference materials analysed during the course of this study can be found in Halama *et al.* (2010, 2014). The analytical uncertainties for N concentrations are usually <5%. For $\delta^{15}N$ values (referenced to the isotopic composition of

atmospheric N_2, "air"), uncertainties are 0.15‰ (1σ) for samples with > 5 µg/g N and 0.6‰ (1σ) for samples with 1-5 µg/g N.

3.2. Major and trace elements

Major and trace element data of the JTS and FTS traverses were published in Beinlich *et al.* (2010) and van der Straaten *et al.* (2012), respectively, and are reproduced in the supplemental dataset. Major and trace elements of the Vendée traverse (supplemental dataset) were analysed by X-ray fluorescence at Universität Heidelberg using a Siemens® SRS303 instrument equipped with a Rh-tube. Major and minor elements were measured on fused glass discs with an accuracy of 0.5-1%. Trace elements (Cr, Ni, Sr, Zr, Ba) were measured on pressed pellets with an accuracy of 5-10%. Further details about the XRF methods are given in Pauly *et al.* (2016). Lithium concentrations were determined at the University of Bristol with a sample-standard bracketing technique using a ThermoElectron®Neptune MC-ICP-MS as described in Marschall *et al.* (2007b). Concentrations were determined by intensity comparison with the bracketing standard (NIST L-SVEC) and have a precision of approximately ±10%.

4. Results

In the profile representing the prograde blueschist-eclogite transformation (JTS sequence), N concentrations successively decrease from the host blueschist (~26 µg/g) to the blueschist-eclogite transition zone (BETZ; 19-23 µg/g) and the eclogitic selvage (12-16 µg/g; Figure 3a). The quartz-carbonate vein has the lowest N concentrations (9.5 µg/g) and the highest $\delta^{15}N_{air}$ value (+4.8‰) in this sequence (Table 1). Nitrogen isotopic compositions of the eclogitic selvage ($\delta^{15}N$ = +2.6 ± 0.2‰) are slightly elevated compared to the BETZ (+2.0 ± 0.2‰) and the host blueschists ($\delta^{15}N$ = +1.8 to +2.3‰). Overall, the profile shows a systematic decrease in [N] from the host wall rock towards the vein, which is paralleled by LILE such as Rb (Figure 3a; supplemental dataset). Excluding the vein, the overall range in $\delta^{15}N$ in eclogites and blueschists is very limited (only about 1‰) with an average of +2.1±0.3‰ (n=9).

In the profile representing the retrograde eclogite-blueschist transition (FTS sequence), there is a broad increase in N contents from the eclogite towards the blueschist, but the trend shows significant scatter and there is also variability between adjacent samples from the same drill core (3.1-3A and 3.1-3B). The overall range in N contents (8-27 µg/g) is comparable to the JTS

sequence, but the variability in $\delta^{15}N$ is larger ($\delta^{15}N$ = +1.0 to +5.4‰). $\delta^{15}N$ varies unsystematically with regard to distance along the profile (Table 1).

In the eclogite-gneiss profile, the country rock gneisses have high N contents (14-52 µg/g) and positive $\delta^{15}N$ values (+2.9 to +5.8‰; Table 1). $\delta^{15}N$ values of both garnet amphibolites and eclogites are within the range of the gneiss values, but [N] becomes increasingly lower towards the eclogite with 11-24 µg/g for the amphibolites and 10-14 µg/g for the retrogressed eclogite (Figure 3b). The pristine eclogite is characterized by the lowest N concentrations (2.1-3.6 µg/g) and the lightest N isotopic compositions ($\delta^{15}N$ = +2.1 to +3.6‰). The elements Ba and Li show a similar behaviour as N with successively decreasing concentrations from the gneisses to the eclogites (Figure 3b; supplemental dataset).

[Figure 3 near here]
[Table 1 near here]

5. Discussion

5.1. Residency of nitrogen

Nitrogen occurs as ammonium (NH_4^+) in most silicate minerals, where it substitutes for K^+ due to the similarity of these ions in charge and ionic radius. NH_4^+ is thus most strongly concentrated in micas and alkali feldspars in many crustal rocks (Honma and Itihara 1981), as reflected by correlations of N contents with concentrations of LILE (K, Rb, Cs, Ba) in several metasedimentary suites (Bebout *et al.* 1999; Busigny *et al.* 2003; Sievers *et al.* 2016, this issue). Phengite (Si-rich potassic white mica) is the main N carrier mineral in high-*P/T* metamorphosed mafic and ultramafic rocks, but NH_4^+ may also occur in Ca-Na minerals where phengite is absent (Busingy *et al.*, 2011; Halama *et al.*, 2010; 2012). The positive correlation of N with K, Ba, Rb and Cs (Figure 4) in both Tianshan sequences points to a mineralogical control by phengite regarding the N concentrations in the bulk rocks, because phengite is known to be the principal carrier for these elements in phengite-bearing eclogites and high-*P/T* metapelites (e.g., Sorensen *et al.* 1997; Zack *et al.* 2001).

The JTS sequence shows the most striking correlation among N abundances and LILE concentrations, with a systematic decrease from host blueschists via the BETZ towards eclogites and the vein (Figure 4a). The key role of phengite as N host is underlined by the decreasing modal

occurrence of white mica (phengite + paragonite) towards the vein (Figure 5; Beinlich *et al.* 2010). The somewhat larger scatter in the FTS sequence (Figure 4b) may be related to the generally much smaller concentration variations compared to the JTS sequence. Moreover, paragonite (sodic white mica) forms in response to the retrograde overprint in the FTS sequence. Although paragonite is capable of incorporating significant amounts of N in the order of up to 100 μg/g (Busigny *et al.* 2011), phengite frequently contains several hundreds of μg/g (Sadofsky and Bebout 2000) and is hence a more likely major N host. The unsystematic variations in modal abundances of these two phases are therefore thought to contribute to the scattered trends in the FTS sequence. In the eclogite-gneiss profile, there is a systematic, coupled increase in N and LILE as well as Li from eclogites via retrogressed eclogites and amphibolites towards the surrounding gneisses (Figure 4c). The low N contents in the eclogites are consistent with the lack of K-bearing phases. Any N present is probably residing in omphacitic (Na-Ca) clinopyroxene, in agreement with observations from natural metagabbros (Busigny *et al.* 2011) and experimental results that show the potential of clinopyroxene to incorporate N at ultrahigh pressures (Watenphul *et al.* 2010). Additional N present in retrogressed eclogites and amphibolites may be incorporated into plagioclase, for which N concentrations of 2-45 μg/g have been reported, substituting for Ca and Na (Honma and Itihara 1981), and to a lesser degree into amphibole (2-5 μg/g N, Honma and Itihara 1981). In the gneisses, N can be incorporated into muscovite and biotite, both of which can host large amounts (>1000 μg/g) of N (Sadofsky and Bebout 2000).

[Figure 4 near here]
[Figure 5 near here]

5.2. Nitrogen elemental and isotopic characteristics

All three of the sample suites are characterized by a limited (≤ 5‰) variation in $\delta^{15}N$ and positive $\delta^{15}N$ values, which distinguishes them from fresh MORB (Figure 6). Most of the $\delta^{15}N$ values of the mafic samples overlap with those of global eclogites, which were interpreted to largely reflect the N isotope compositions of their protolith (altered oceanic crust, AOC) with or without the effects of metamorphic dehydration (Halama *et al.* 2010). Metamorphic dehydration generally causes a decrease in N concentrations and an increase in $\delta^{15}N$ values (Haendel *et al.* 1986; Bebout and Fogel 1992), but the large compositional variability of AOC hinders the identification

of dehydration effects. At each location, some of the mafic samples have elevated N contents relative to global eclogites, in particular the Tianshan blueschists and the Vendée amphibolites, trending towards compositions of metasediments (Figure 6). In the prograde blueschist-eclogite JTS sequence, the blueschists represent the rocks least affected by eclogitization-causing fluid overprint, and hence may have inherited their signature during a previous metasomatic event, e.g. during seafloor alteration or blueschist-facies metamorphism. The trend in the JTS sequence towards relatively N-poor compositions is unlikely to be entirely due to a decreasing modal abundance of white mica as suitable host mineral for N because the modal abundances of white mica are similar in the host blueschists (8-11%) and the BETZ (12-15%), with only the eclogitic selvage having lower contents (4-11%; Beinlich *et al.* 2010). Hence, the trend suggests that the fluid inducing the eclogitization was relatively poor in N and probably not of sedimentary origin. This finding is in agreement with the Ca and Sr isotope data pointing to a dehydrating oceanic lithosphere, i.e. AOC or serpentinized slab mantle, as potential fluid source (John *et al.*, 2012). An estimate for the average $\delta^{15}N$ of ultramafic rocks recycled into the mantle is +3±2‰ (Halama *et al.* 2014), but individual serpentinized peridotite samples have even more positive $\delta^{15}N$ values of up to +15‰ (Philippot *et al.* 2007).

In contrast, the blueschists of the FTS sequence are among the samples that are most strongly affected by retrograde metasomatism. Their elevated N contents at moderately positive $\delta^{15}N$ are consistent with a metasomatic overprint by a fluid that either originated from or equilibrated with metasedimentary rocks. In the Vendée profile, the field evidence clearly demonstrates increasing fluid-induced overprint of the eclogite lens by fluids derived from the surrounding metasedimentary gneisses, producing the sequence fresh eclogite – retrogressed eclogite – amphibolite – metasedimentary gneiss. This profile allows evaluation of the effects of the metasedimentary fluids on [N] and $\delta^{15}N$ in the eclogite lens. Both the N concentrations and the $\delta^{15}N$ values increase in the metasomatically overprinted mafic rocks compared to the pristine eclogite. These features can be explained by assuming that the country rock paragneisses with high N contents and an adequate N isotopic composition were the source lithology for the metasomatic fluids, corroborating the field evidence. Hence, both the Tianshan FTS and the Vendée profile underline the sensitivity of the N system to sediment-derived fluids. These fluids incorporated biogenic N that was originally present as organic matter in the sediments. Granitic rocks from the Cornubian batholith similarly show high N contents (6-139 µg/g) and positive $\delta^{15}N$ (+5 to +10‰) values (Boyd *et al.* 1993). These features were interpreted to reflect inheritance of N of biological origin as the granites are essentially derived from the anatexis of NH_4^+-bearing metasediments that originally contained organic material (Hall 1987; Boyd *et al.* 1993).

[Figure 6 near here]

5.3. Fluid-rock interaction processes

In this section, we focus on the prograde blueschist-eclogite JTS sequence because it shows a relatively simple mineralogical control on N contents, resulting in clear correlations that can be compared to various fluid-rock interaction processes potentially affecting the rocks. Busigny and Bebout (2013) summarized four types of N exchange between mineral and fluid that can be distinguished during metamorphism, and each of these will be evaluated in turn:

(1) Thermal decomposition: Thermal decomposition causes the complete breakdown of mineral hosts due to increasing temperatures and the onset of partial melting. This leads to a decreasing modal abundance of mica and loss of N if no other suitable host phases for N, such as K-feldspar (incorporation of NH_4^+) or cordierite (incorporation of N_2 in channels of the mineral structure), are present in the melting residue (Palya *et al.* 2011). Thermal decomposition can be excluded in the studied profiles because there is no field or petrographic evidence for partial melting and estimates of peak temperatures are too low for partial melting of mafic rocks to occur.

(2) Cation exchange: Cation exchange of NH_4^+ and K^+ between white mica and a fluid can release NH_4^+ into the fluid if the rock equilibrates with a fluid rich in K^+, thereby replacing NH_4^+ in white mica by K^+ (Eugster and Munoz 1966; Busigny and Bebout 2013). A similar exchange may occur between NH_4^+ and Rb^+ or Cs^+. This process is expected to cause a negative correlation of NH_4^+ with K^+ (and Rb^+, Cs^+). However, all investigated profiles show a positive correlation of K and N. This is the opposite behaviour to what would be expected if cation exchange was the dominant fluid-rock interaction process and we hence exclude cation exchange as major process.

(3) Continuous metamorphic devolatilization reactions: Devolatilization reactions during prograde metamorphism cause changes in mica chemistry and mica modal abundances in the rock (Bebout and Fogel 1992; Bebout *et al.* 2013). During devolatilization, isotopically light N is preferentially fractionated into the metamorphic fluid. Consequently, residual mica records an increase in $\delta^{15}N$ with increasing degrees of devolatilization (Haendel *et al.* 1986; Bebout and Fogel 1992; Jia *et al.*

2006). To test the effects of metamorphic devolatilization, we calculated the composition of the residual rock for batch devolatilization and Rayleigh distillation models (Figure 7a). In an open-system Rayleigh distillation model, each fluid increment produced by phengite dehydration is immediately removed from the rock. In contrast, the batch devolatilization model assumes that all of the fluid released equilibrates with the rock and is lost in a single batch (Valley 1986).

The isotopic fractionation depends on the N speciation in the fluid (N_2 or NH_3). It is evident that devolatilization models involving NH_3 cannot explain the observed trend in the JTS sequence (Figure 7a). Busigny *et al.* (2003) modelled phengite chemical evolution during progressive Rayleigh distillation for LILE, and we use this approach to test the applicability of continuous metamorphic reactions on the prograde blueschist-eclogite JTS data set (Figure 7b, c). Different partition coefficients between fluid and phengite for K, Rb, Cs and N cause fractionation between these elements during devolatilization (Melzer and Wunder 2000; Busigny *et al.* 2003). Since all these elements predominantly resided in phengite, their ratios in phengite reflect those of the whole rock (Zack *et al.* 2001). Caesium has a larger preference for the fluid than both Rb and N, producing a relatively sharp decrease in Cs abundances and curved Rayleigh distillation trends in bivariate diagrams (Figure 7b, c). The linear correlations of the measured data suggest that continuous metamorphic phengite dehydration via a Rayleigh distillation process in an open system cannot have caused the coupled decrease in Rb-Cs and N-Cs, respectively. The coupled losses of these elements which are observed with decreasing distance to the vein do not appear to obey a K_d-controlled Rayleigh distillation process. However, a good fit to the JTS data is obtained for a N_2 batch devolatilization model, only the vein plots off the modelled trend (Figure 7a). Hence, the N isotope data support a batch devolatilization process.

[Figure 7 near here]

(4) Fluid-induced breakdown of white mica: It has been shown that the eclogitization adjacent to the vein structure occurred due to fluid-mediated replacement processes during which the blueschist continuously equilibrated with an external fluid characterized by a composition that differed strongly from that of the wall rock blueschist (Beinlich *et al.* 2010; John *et al.* 2012). Consequently, the blueschist mineral assemblage has been successively replaced by a new eclogite assemblage (Putnis and Austrheim 2010; Putnis and John 2010). This process can be generalised by breakdown reactions such as:

$$2\ KAl_2(Si_3AlO_{10})(OH)_2 + 2\ H^+ = 3\ Al_2SiO_5 + 3\ SiO_2 + 2\ K^+ + 3\ H_2O \quad [1]$$

$$2\ KAl_2(Si_3AlO_{10})(OH)_2 = 3\ Al_2SiO_5 + 3\ SiO_2 + 2\ K^+ + 2\ OH^- + H_2O \quad [2]$$

Once liberated from phengite, N and the LILE (formerly substituting for K in phengite) enter the fluid, which mediates diffusive or advective transport towards the nearest transport vein leading to long-distance element removal (Zack and John 2007). This process of fluid-induced decomposition of white mica is in agreement with the coupled bulk losses of LILE and N. The combined stripping of LILE and N from the blueschists requires infiltration of a K-poor fluid, which drives chemical reactions towards reduced chemical potential gradients for fluid species by destroying phengite and releasing LILE and N into the fluids (Breeding *et al.* 2004; John *et al.* 2012). Loss of Al_2O_3 in both the BETZ (~2-9%) and in the eclogitic selvage (~12%) compared to the blueschist host (Beinlich *et al.* 2010) suggest release and removal of Al during phengite breakdown. The behaviour of Si is less systematic, with some relative losses in BETZ samples but also gains in the eclogitic selvage (Beinlich *et al.* 2010), likely related to infiltration from the vein-forming fluid.

If the fluids infiltrating the rock are highly oxidising, NH_4^+ will be partially oxidised to N_2, which will then be lost from the system in the fluid (Bebout and Fogel 1992; Svensen *et al.* 2008). Oxidizing fluids are capable of destroying ammonium muscovite and forming kyanite and quartz by the reaction (Eugster and Munoz 1966):

$$2\ NH_4Al_2(Si_3AlO_{10})(OH)_2 + 1.5\ O_2 = 3\ Al_2SiO_5 + 3\ SiO_2 + N_2 + 6\ H_2O \quad [3]$$

More reducing fluids may cause breakdown of ammonium muscovite by the reaction

$$2\ NH_4Al_2(Si_3AlO_{10})(OH)_2 = 3\ Al_2SiO_5 + 3\ SiO_2 + 2\ NH_3 + 3\ H_2O \quad [4]$$

Generally, fluid-rock interaction can be considered as an important mechanism to release large amounts of specific elements that are hosted by a single mineral phase. Regarding the transport of LILE and N, phengite mode and breakdown rate are the most important parameters of the rock for storage and release, respectively, of these elements. The combined N elemental and isotope systematics suggest a scenario of fluid-induced breakdown of white mica and batch devolatilization of N in the system.

5.4. Transfer and sources of nitrogen

The prograde blueschist-eclogite transition of the JTS sequence, which is induced by metasomatism, provides compelling evidence for removal of N due to phengite breakdown. Other elements, such as Ca, Sr and Pb, were added by the fluid-induced overprint (Beinlich *et al.* 2010), and consequently exhibit negative correlations with N contents (Figure 8). The degree to which N

potentially present in the fluid would have been able to exchange with the rock and alter [N] and $\delta^{15}N$ depends on the compatibility of N in the available mineral hosts and the abundance of these host phases. In the metasomatically formed eclogites of the JTS sequence, no other mineral except phengite is able to incorporate significant amounts of N. The $\delta^{15}N_{fluid}$ is estimated as ~ +7‰ based on vein composition and the NH_4^+-N_2 fractionation factor at 527°C from Hanschmann (1981). Positive $\delta^{15}N$ that overlap the vein composition were observed in AOC from the East Pacific Rise (Busigny *et al.* 2005) and in various (meta)sedimentary rocks (Figure 9a). However, the combination of a high-$\delta^{15}N$ fluid that introduced large amounts of externally-derived Ca and Sr, but not LILE, is pointing towards AOC rather than (meta)sediments as the most likely fluid source. This conclusion is consistent with Ca-Sr isotope data, which demonstrated that seawater-altered lithospheric rocks were the dominant source for the metasomatic fluid that induced eclogitization in the JTS sequence (John *et al.* 2012). In the $\delta^{15}N$ – Rb/N diagram (Figure 9a), where mixing relationships appear as straight lines, an apparent mixing trend between the JTS rock with the highest Rb/N ratio and the vein composition yields a decent fit to the data points. Our preferred interpretation of this apparent mixing relationship is that up to ~40% of the initially present phengite was destroyed by the fluid-induced overprint, in agreement with the observed decrease of modal phengite abundance (Beinlich *et al.* 2010), causing successively decreasing Rb/N ratios coupled to decreasing N contents. Changes in $\delta^{15}N$ in the overprinted eclogites compared to the blueschists are minor and an externally-derived N isotope signature is not clearly discernible from $\delta^{15}N$ variability due to protolith heterogeneities ± devolatilization effects.

In contrast to the JTS sequence, both of the two profiles with a retrograde overprint, the FTS sequence and the Vendée profile, show addition of N during metasomatism. For the FTS sequence, the addition was not pervasive and systematic, as the [N]-distance relationships are scattered, possibly related to the availability of fluid pathways within the rock and/or small-scale heterogeneities. The straight line correlation on the $\delta^{15}N$ – Rb/N diagram (Figure 9a) points to a mixing relationship, but the position of both eclogite and blueschist at the upper end of this trend add a complexity likely related to the co-existence of phengite and paragonite, which precludes any further conclusions.

Retrograde alteration in the Vendée mafic rocks was accompanied by increasing K/N ratios and $\delta^{15}N$ values (Figure 9b). Any metasomatic fluid entering the eclogite lenses must have passed through the surrounding paragneisses, which therefore constitute the most likely source for any elements added to the eclogites. Retrogressed eclogites and amphibolites are enriched in N up to 10 times compared to the precursor eclogites and $\delta^{15}N$ has been changed by up to 4‰. Original protolith signatures and effects of prograde metamorphism were overprinted by the retrograde

501 metamorphism as N has been transported on length scales of at least several 10s of meters, although
502 the most pristine eclogites may still preserve the original signatures. The contribution by the
503 relatively N-rich, high-$\delta^{15}N$ paragneisses is exemplified by mixing relationships between two
504 different gneisses and eclogite where the whole-rock K/N ratios are considered to approximate
505 those of the fluid (Figure 9b). Given the large spread in K/N ratios in the gneisses, fluid-mediated
506 mixing can easily explain elevated K/N in retrograde overprinted eclogites. The complete overlap in
507 $\delta^{15}N$ between retrogressed eclogites/amphibolites and gneisses provides evidence for the great
508 sensitivity of the N isotope system to fluids that interacted with or are derived from
509 (meta)sediments. Amphibolites and retrogressed eclogites have isotopically almost fully
510 equilibrated with the gneisses, and heterogeneities, inherited from the eclogite precursor, were only
511 preserved in the inner parts of the eclogite lens. The fluid-mediated influx of N from the gneisses
512 into the eclogite lens was likely aided by transport of N via amphibole veins, which occur in the
513 eclogites and served as more effective transport pathway compared to the less permeable bulk rock.
514 The Vendée profile not only shows direct evidence for the derivation of N in a metasomatic fluid
515 from metasedimentary rocks, but, importantly, that this process can happen on length scales of 10s
516 of meters.
517
518
519 [Figure 8 near here]
520 [Figure 9 near here]
521
522
523 ## 6. Conclusions
524
525 We investigated three profiles in metasomatically overprinted high-pressure metamorphic rocks
526 to determine the effects of fluid-rock interaction on N elemental and isotopic systematics. Positive
527 correlations of N with K, Ba, Rb and Cs in blueschists and eclogites demonstrate that phengitic
528 white mica is the major N host in metamorphic rocks with mafic precursors. During prograde
529 overprint of blueschists and transformation into eclogites, the observed straight line correlations
530 between N and LILE and near-constant ratios of N/K, N/Rb, N/Cs and Cs/Rb do not resemble
531 differential losses related to differing equilibrium partitioning during metamorphic devolatilization
532 via a Rayleigh distillation process, but instead indicate that fluid-mediated N mobilization and loss
533 from the rock is related to complete breakdown of white mica. Hence, N abundances are strongly
534 controlled by the stability and presence of white mica in HP metamorphic rocks, and external N

contributions to the whole rock budget remain insignificant as long as no other N host forms. Fluid-induced breakdown of phengite in HP rocks can liberate large amounts of N that is released into the fluid (Figure 10). The N isotopic compositions show only small variations that are consistent with a batch devolatilization process coupled to the phengite breakdown. During fluid-induced retrograde overprint of eclogites, the N system is highly sensitive to fluids that equilibrated with metasedimentary rocks and can be used to trace the extent of N transport from host rocks into eclogite lenses. This transport can occur over several tens of meters and affect both N concentrations and isotopic compositions (Figure 10), as evidenced by a profile from metasedimentary gneisses into an eclogite lens. Elevated N contents in retrogressed mafic HP rocks suggest that plagioclase and amphibole are capable to incorporate N derived from metasomatic fluids.

[Figure 10 near here]

Acknowledgements

HRM would like to thank Gaston Godard for field guidance in the Vendée. Lithium concentration data were previously unpublished and were provided by Philip Pogge von Strandmann, which is gratefully acknowledged. We thank Sarah Penniston-Dorland and Vincent Busigny for the constructive reviews that helped to greatly improve the manuscript. Support of this project was partly provided by National Science Foundation grant EAR-0711355 to GEB.

557 **References**

558

559 Bebout, G.E., 1997, Nitrogen isotope tracers of high-temperature fluid-rock interactions: Case study
560 of the Catalina Schist, California: Earth and Planetary Science Letters, v. 151, p. 77-90.
561 Bebout, G.E., 2007, Metamorphic chemical geodynamics of subduction zones: Earth and Planetary
562 Science Letters, v. 260, p. 373-393.
563 Bebout, G.E., 2014, Chemical and isotopic cycling in subduction zones, *in* Rudnick, R. L., ed.,
564 Treatise on Geochemistry: The Crust, 2nd ed., Volume 3, Elsevier, p. 703-747.
565 Bebout, G.E., Agard, P., Kobayashi, K., Moriguti, T., and Nakamura, E., 2013, Devolatilization
566 history and trace element mobility in deeply subducted sedimentary rocks: Evidence from
567 Western Alps HP/UHP suites: Chemical Geology, v. 342, p.1-20.
568 Bebout, G.E., and Fogel, M.L., 1992, Nitrogen-isotope compositions of metasedimentary rocks in
569 the Catalina Schist, California: Implications for metamorphic devolatilization history:
570 Geochimica et Cosmochimica Acta, v. 56, p. 2839-2849.
571 Bebout, G.E., Idleman, B.D., Li, L., and Hilkert, A., 2007, Isotope-ratio-monitoring gas
572 chromatography methods for high-precision isotopic analysis of nanomole quantities of silicate
573 nitrogen: Chemical Geology, v. 240, p. 1-10.
574 Bebout, G.E., Lazzeri, K.E., and Geiger, C.A., 2016, Pathways for nitrogen cycling in Earth's crust
575 and upper mantle: A review and new results for microporous beryl and cordierite: American
576 Mineralogist, v. 101, p. 7-24.
577 Bebout, G.E., and Penniston-Dorland, S.C., 2016, Fluid and mass transfer at subduction interfaces –
578 The field metamorphic record: Lithos, v. 240-243, p. 228-258.
579 Beinlich, A., Klemd, R., John, T., and Gao, J., 2010, Trace-element mobilization during Ca-
580 metasomatism along a major fluid conduit: Eclogitization of a blueschist as a consequence of
581 fluid-rock interaction: Geochimica et Cosmochimica Acta, v. 74, p. 1892-1922.
582 Bernard-Griffiths, J., and Cornichet, J., 1985, Origin of eclogites from South Brittany, France: A
583 Sm-Nd isotopic and REE study: Chemical Geology (Isotope Geoscience Section), v. 52, p. 185-
584 201.
585 Boyd, S.R., Hall, A., and Pillinger, C.T., 1993, The measurement of $\delta^{15}N$ in crustal rocks by static
586 vacuum mass spectrometry: Application to the origin of the ammonium in the Cornubian
587 batholith, southwest England: Geochimica et Cosmochimica Acta, v. 57, p. 1339-1347.
588 Breeding, C.M., Ague, J.J., and Bröcker, M., 2004, Fluid-metasedimentary rock interactions in
589 subduction-zone mélange: Implications for the chemical composition of arc magmas: Geology,
590 v. 32, p. 1041-1044.

591 Busigny, V., and Bebout, G. E., 2013, Nitrogen in the Silicate Earth: Speciation and isotopic
592 behavior during mineral-fluid interactions: Elements, v. 9, p. 353-358.
593 Busigny, V., Cartigny, P., Philippot, P., Ader, M., and Javoy, M., 2003, Massive recycling of
594 nitrogen and other fluid-mobile elements (K, Rb, Cs, H) in a cold slab environment: evidence
595 from HP to UHP oceanic metasediments of the Schistes Lustrés nappe (western Alps, Europe):
596 Earth and Planetary Science Letters, v. 215, p. 27-42.
597 Busigny, V., Cartigny, P., and Philippot, P., 2011, Nitrogen isotopes in ophiolitic metagabbros: A
598 re-evaluation of modern nitrogen fluxes in subduction zones and implication for the early Earth
599 atmosphere: Geochimica et Cosmochimica Acta, v. 75, p. 7502-7521.
600 Busigny, V., Laverne, C., and Bonifacie M., 2005, Nitrogen content and isotopic composition of
601 oceanic crust at a superfast spreading ridge: A profile in altered basalts from ODP Site 1256, Leg
602 206: Geochemistry Geophysics Geosystems, v. 6, Q12O01, doi:10.1029/2005GC001020.
603 Dauphas, N., and Marty, B., 1999, Heavy nitrogen in carbonatites of the Kola Peninsula: A possible
604 signature of the deep mantle: Science, v. 286, p. 2488-2490.
605 Elkins, L. J., Fischer, T. P., Hilton, D. R., Sharp, Z. D., McKnight, S., and Walker, J., 2006, Tracing
606 nitrogen in volcanic and geothermal volatiles from the Nicaraguan volcanic front. Geochimica et
607 Cosmochimica Acta, v. 70, p. 5215-5235.
608 Eugster, H.P., and Munoz, J., 1966, Ammonium micas: possible sources of atmospheric ammonia
609 and nitrogen: Science, v. 151, p. 683-686.
610 Gao, J., and Klemd, R., 2001, Primary fluids entrapped at blueschist to eclogite transition: evidence
611 from the Tianshan meta-subduction complex in northwest China: Contributions to Mineralogy
612 and Petrology, v. 142, p. 1-14.
613 Gao, J., and Klemd, R., 2003, Formation of HP-LT rocks and their tectonic implications in the
614 western Tianshan orogen, NW China; geochemical and age constraints: Lithos, v. 66, p. 1–22.
615 Gao, J., John, T., Klemd, R., and Xiong, X., 2007, Mobilization of Ti-Nb-Ta during subduction:
616 evidence from rutile-bearing dehydration segregations and veins hosted in eclogite, Tianshan,
617 NW China: Geochimica et Cosmochimica Acta, v. 71, p. 4974-4996.
618 Gao, J., Klemd, R., Zhang, L., Wang, Z., and Xiao, X., 1999, P-T path of high-pressure/low-
619 temperature rocks and tectonic implications in the western Tian Shan mountains, NW China:
620 Journal of metamorphic Geology, v. 17, p. 621-636.
621 Gao, J., Li, M., He, G., and Xiao, X., 1998, Paleozoic tectonic evolution of the Tianshan Orogen,
622 northwestern China: Tectonophysics, v. 287, p. 213-231.
623 Gao, J., Long, L.L., Klemd, R., Qian, Q., Liu, D.Y., Xiong, X.M., Su, W., Wang, Y.T., and Yang,
624 F.Q., 2009, Tectonic evolution of the South Tianshan orogen and adjacent regions, NW China:

625 geochemical and age constraints of granitoid rocks: International Journal of Earth Sciences, v.
626 98, p. 1221–1238.
627 Godard, G., 2009, Two orogenic cycles recorded in eclogite-facies gneiss from the southern
628 Armorican Massif (France), European Journal of Mineralogy, v. 21, p. 1173-1190.
629 Haendel, D., Mühle, K., Nitzsche, H.-M., Stiehl, G., and Wand, U., 1986, Isotopic variations of the
630 fixed nitrogen in metamorphic rocks: Geochimica et Cosmochimica Acta, v. 50, p. 749-758.
631 Halama, R., Bebout, G.E., John, T., and Schenk, V., 2010, Nitrogen recycling in subducted oceanic
632 lithosphere: The record in high- and ultrahigh-pressure metabasaltic rocks: Geochimica et
633 Cosmochimica Acta, v. 74, p. 1636-1652.
634 Halama, R., Bebout, G.E., John, T., and Scambelluri, M., 2014, Nitrogen recycling in subducted
635 mantle rocks and implications for the global nitrogen cycle: International Journal of Earth
636 Sciences, v. 103, p. 2081-2099.
637 Halama, R., John, T., Herms, P., Hauff, F., and Schenk, V., 2011, A stable (Li, O) and radiogenic
638 (Sr, Nd) isotope perspective on metasomatic processes in a subducting slab: Chemical Geology,
639 v. 281, p. 151-166.
640 Hall, A., 1987, The ammonium content of Caledonian granites: Journal of the Geological Society of
641 London, 144, 671-674.
642 Hanschmann, G., 1981, Berechnung von Isotopieeffekten auf quantenchemischer Grundlage am
643 Beispiel stickstoffhaltiger Moleküle: ZFI-Mitteilungen, v. 41, v. 19-31.
644 Honma, H., and Itihara, Y., 1981, Distribution of ammonium in minerals of metamorphic and
645 granitic rocks: Geochimica et Cosmochimica Acta, v. 45, p. 983-988.
646 Jia, Y., 2006, Nitrogen isotope fractionations during progressive metamorphism: A case study from
647 the Paleozoic Cooma metasedimentary complex, southeastern Australia: Geochimica et
648 Cosmochimica Acta, v. 70, p. 5201-5214.
649 John, T., Gussone, N., Podladchikov, Y.Y., Bebout, G.E., Dohmen, R., Halama, R., Klemd, R.,
650 Magna, T., and Seitz, H.-M., 2012, Volcanic arcs fed by rapid pulsed fluid flow through
651 subducting slabs: Nature Geoscience, v. 5, p. 489-492.
652 John, T., Klemd, R., Gao, J., and Garbe-Schönberg, C.D., 2008, Trace-element mobilization in
653 slabs due to non steady-state fluid–rock interaction: constraints from an eclogite-facies transport
654 vein in blueschist (Tianshan, China): Lithos, v. 103, p. 1–24.
655 John, T., Scambelluri, M., Frische, M., Barnes, J.D., and Bach, W., 2011, Dehydration of
656 subducting serpentinite: Implications for halogen mobility in subduction zones and the deep
657 halogen cycle: Earth and Planetary Science Letters, v. 308, p. 65-76.

John, T., Scherer, E.E., Haase, K., and Schenk, V., 2004, Trace element fractionation during fluid-induced eclogitization in a subducting slab: trace element and Lu-Hf-Sm-Nd isotope systematics: Earth and Planetary Science Letters, v. 227, p. 441-456.

Johnson, B., and Goldblatt, C., 2015, The nitrogen budget of Earth: Earth-Science Reviews, v. 148, p. 150-173.

Klemd, R., Schröter, F.C., Will, T.M., and Gao, J., 2002, P-T evolution of glaucophane-omphacite bearing HP-LT rocks in the western Tianshan Orogen, NW China; new evidence for Alpine-type tectonics: Journal of metamorphic Geology, v. 20, p. 239-254.

Klemd, R., Bröcker, M., Hacker, B.R., Gao, J., Gans, P., and Wemmer, K., 2005, New age constraints on the metamorphic evolution of the high-pressure/low-temperature belt in the western Tianshan mountains, NW China: Journal of Geology, v. 113, p. 157–168.

Klemd, R., John, T., Scherer, E.E., Rondenay, S., and Gao, J., 2011, Change in dip of subducting slabs at greater depths: petrological and geochronological evidence from HP-UHP rocks (Tianshan, NW-China): Earth and Planetary Science Letters, v. 310, p. 9-20.

Konrad-Schmolke, M., and Halama, R., 2014, Combined thermodynamic-geochemical modeling in metamorphic geology: Boron as tracer of fluid-rock interaction: Lithos, v. 208-209, p. 393-414.

Li, L., and Bebout, G. E., 2005, Carbon and nitrogen geochemistry of sediments in the Central American convergent margin: Insights regarding subduction input fluxes, diagenesis, and paleoproductivity: Journal of Geophysical Research, v. 110 (B11202), doi:10.1029/2004JB003276.

Li, L., Bebout, G. E., and Idleman, B. D., 2007, Nitrogen concentration and $\delta^{15}N$ of altered oceanic crust obtained on ODP Legs 129 and 185: Insights into alteration-related nitrogen enrichment and the nitrogen subduction budget: Geochimica et Cosmochimica Acta, v. 71, p. 2344-2360.

Li, L., Zheng, Y.-F., Cartigny, P., and Li, J., 2014, Anomalous nitrogen isotopes in ultrahigh-pressure metamorphic rocks from the Sulu orogenic belt: Effect of abiotic nitrogen reduction during fluid–rock interaction: Earth and Planetary Science Letters, v. 403, p. 67-78.

Lü, Z., Zhang, L., Du, J., and Bucher, K., 2008, Coesite inclusions in garnet from eclogitic rocks in western Tianshan, northwest China: Convincing proof of UHP metamorphism: American Mineralogist, v. 93, p. 1845-1850.

Lü, Z., Zhang, L., Du, J., and Bucher, K., 2009, Petrology of coesite-bearing eclogite from Habutengsu Valley, western Tianshan, NW China and its tectonometamorphic implication: Journal of metamorphic Geology, v. 27, p. 773-787.

690 Marschall, H.R., Altherr, R., and Rüpke, L., 2007a, Squeezing out the slab – modelling the release
691 of Li, Be and B during progressive high-pressure metamorphism: Chemical Geology, v. 239, p.
692 323-335.
693 Marschall, H.R., Pogge von Strandmann, P.A.E., Seitz, H.-M., Elliott, T., and Niu, Y., 2007b, The
694 lithium isotopic composition of orogenic eclogites and deep subducted slabs: Earth and Planetary
695 Science Letters, v. 262, p. 563-580.
696 Marty, B., and Dauphas, N., 2003, The nitrogen record of crust-mantle interaction and mantle
697 convection from Archean to Present: Earth and Planetary Science Letters, v. 206, p. 397-410.
698 Matte, P., 2001, The Variscan collage and orogeny (480-290 Ma) and the tectonic definition of the
699 Armorica microplate: a review: Terra Nova, v. 13, p. 122-128.
700 Mauler, A., Godard, G., and Kunze, K., 2001, Crystallographic fabrics of omphacite, rutile and
701 quartz in Vendée eclogites (Armorican Massif, France). Consequences for deformation
702 mechanisms and regimes: Tectonophysics, v. 342, p. 81-112.
703 Melzer, S., and Wunder, B., 2000, Island-arc basalt alkali ratios: Constraints from phengite-fluid
704 partitioning experiments: Geology, v. 28, p. 583-586.
705 Mikhail, S., and Howell, D., 2016, A petrological assessment of diamond as a recorder of the
706 mantle nitrogen cycle: American Mineralogist, v. 101, p. 780-787.
707 Mingram, B., and Bräuer, K., 2001, Ammonium concentration and nitrogen isotope composition in
708 metasedimentary rocks from different tectonometamorphic units of the European Variscan Belt:
709 Geochimica et Cosmochimica Acta, v. 65, p. 273-287.
710 Palya, A.P., Buick, I.S., and Bebout, G.E., 2011, Storage and mobility of nitrogen in the continental
711 crust: Evidence from partially melted metasedimentary rocks, Mt. Stafford, Australia: Chemical
712 Geology, v. 281, p. 211-226.
713 Pauly, J., Marschall, H.R., Meyer, H.-P., Chatterjee, N., and Monteleone, B., 2016, Prolonged
714 Ediacaran-Cambrian metamorphic history and short-lived high-pressure granulite-facies
715 metamorphism in the H.U. Sverdrupfjella, Dronning Maud Land (East Antarctica): Evidence for
716 continental collision during Gondwana assembly: Journal of Petrology, v. 57, p. 185-228.
717 Peucat, J.J., Vidal, P., Godard, G., and Postaire, B., 1982, Precambrian U-Pb zircon ages in
718 eclogites and garnet pyroxenites from South Brittany (France): an old oceanic crust in the West
719 European Hercynian belt? Earth and Planetary Science Letters, v. 60, p. 70-78.
720 Philippot, P., Busigny, V., Scambelluri, M., and Cartigny, P., 2007, Oxygen and nitrogen isotopes
721 as tracers of fluid activities in serpentinites and metasediments during subduction: Mineralogy
722 and Petrology, v. 91, p. 11-24.

723 Pitcairn, I.K., Teagle, D.A.H., Kerrich, R., Craw, D., and Brewer, T.S., 2005, The behavior of
724 nitrogen and nitrogen isotopes during metamorphism and mineralization: Evidence from the
725 Otago and Alpine Schists, New Zealand: Earth and Planetary Science Letters, v. 233, p. 229-246.
726 Putnis, A., and Austrheim, H., 2010, Fluid-induced processes: metasomatism and metamorphism:
727 Geofluids, v. 10, p. 254-269.
728 Putnis, A., and John, T., 2010, Replacement processes in the Earth's Crust: Elements, v. 6, p. 159-
729 164.
730 Sadofsky S. J., and Bebout, G. E., 2000, Ammonium partitioning and nitrogen-isotope fractionation
731 among coexisting micas during high-temperature fluid-rock interactions: Examples from the
732 New England Appalachians: Geochimica et Cosmochimica Acta, v. 64, p. 2835-2849.
733 Sadofsky, S.J., and Bebout, G.E., 2003, Record of forearc devolatilization in low-T, high-P/T
734 metasedimentary suites: Significance for models of convergent margin chemical cycling:
735 Geochemistry Geophysics Geosystems, v. 4, 9003, doi:10.1029/2002GC000412.
736 Sadofsky, S. J., and Bebout, G. E., 2004, Nitrogen geochemistry of subducting sediments: New
737 results from the Izu-Bonin-Mariana margin and insights regarding global nitrogen subduction:
738 Geochemistry Geophysics Geosystems, v. 5, Q03I15, doi:10.1029/2003GC000543.
739 Şengör, A.C., Natal'in, B.A., and Burtman, V.S., 1993, Evolution of the Altaid tectonic collage and
740 Palaeozoic crustal growth in Eurasia: Nature, v. 364, p. 299–306.
741 Şengör, A.C., and Natal'in, B.A., 1996, Paleotectonics of Asia: fragments of a synthesis, *in*: Yin, A.,
742 and Harrison, M., eds., The tectonic evolution of Asia: Cambridge University Press, Cambridge,
743 p. 486-640.
744 Sievers, N.E., Tenore, J., Bebout, G.E., and Penniston-Dorland, S.C., 2016, Fingerprints of forearc
745 element mobility in blueschist-facies metaconglomerates, Catalina Schist, California:
746 International Geology Review (this issue).
747 Sorensen, S.S., Grossman, J.N., and Perfit, M.R., 1997, Phengite-hosted LILE enrichment in
748 eclogite and related rocks: Implications for fluid-mediated mass transfer in subduction zones and
749 arc magma genesis: Journal of Petrology, v. 38, p. 3-34.
750 Spandler, C., and Pirard, C., 2013, Element recycling from subducting slabs to arc crust: A review:
751 Lithos, v. 170-171, p. 208-223.
752 Su, W., Gao, J., Klemd, R., Li, J.L., Zhang, X., Li, X.H., Chen, N.S., and Zhang, L., 2010, U–Pb
753 zircon geochronology of Tianshan eclogites in NW China: implication for the collision between
754 the Yili and Tarim blocks of the southwestern Altaids: European Journal Mineralogy, v. 22, p.
755 473–478.

Svensen, H., Bebout, G., Kronz, A., Li, L., Planke, S., Chevallier, L., and Jamtveit, B., 2008, Nitrogen geochemistry as a tracer of fluid flow in a hydrothermal vent complex in the Karoo Basin, South Africa. Geochimica et Cosmochimica Acta, v. 72, p. 4929-4947.

Tian, Z.L., and Wei, C.J., 2013, Metamorphism of ultrahigh-pressure eclogites from the Kebuerte Valley, South Tianshan, NW China: phase equilibria and P-T path: Journal of metamorphic Geology, v. 31, p. 281-300.

Valley, J.W., 1986, Stable isotope geochemistry of metamorphic rocks: Reviews in Mineralogy, v. 16, p. 445-489.

van der Straaten, F., Halama, R., John, T., Schenk, V., Hauff, F., and Andersen, N., 2012, Tracing the effects of high-pressure metasomatic fluids and seawater alteration in blueschist-facies overprinted eclogites: Implications for subduction channel processes: Chemical Geology, v. 292-293, p. 69-87.

van der Straaten F., Schenk V., John T., and Gao J., 2008, Blueschist-facies rehydration of eclogites (Tian Shan, NW-China): implications for fluid-rock interaction in the subduction channel: Chemical Geology, v. 225, p. 195-219.

Watenphul, A., Wunder, B., Wirth, R., and Heinrich, W., 2010, Ammonium-bearing clinopyroxene: A potential nitrogen reservoir in the Earth's mantle: Chemical Geology, v. 270, p. 240-248.

Wei, C., Wang, W., Clarke, G.L., Zhang, L., and Song, S., 2009, Metamorphism of high/ultrahigh-pressure pelitic-felsic schist in the South Tianshan orogen, NW China: Phase equilibria and P-T path: Journal of Petrology, v. 50, p. 1973–1991.

Windley, B.F., Allen, M.B., Zhang, C., Zhao, Z.-Y., and Wang, G.-R., 1990, Paleozoic accretion and Cenozoic redeformation of the Chinese Tien Shan Range, central Asia: Geology, v. 18, p. 128–131.

Zack, T., and John, T., 2007, An evaluation of reactive fluid flow and trace element mobility in subducting slabs: Chemical Geology, v. 239, p. 199-216.

Zack, T., Rivers, T., and Foley, S.F., 2001, Cs-Rb-Ba systematics in phengite and amphibole: an assessment of fluid mobility at 2.0 GPa in eclogites from Trescolmen, Central Alps: Contributions to Mineralogy and Petrology, v. 140, p. 651-669.

Figure captions

Figure 1:

Locations and geological setting of the sampling areas. **A)** Simplified geological map of the Chinese South Tianshan (modified after Gao *et al.* 1999). **B)** Geological map showing the Les Essarts HP unit in the Southern Armorican Massif, France (modified after Mauler *et al.* 2001).

Figure 2:

Sketches and field photographs illustrating the sample profiles for **A**) the prograde blueschist-eclogite transition (JTS sequence; Beinlich *et al.* 2010) and **B**) the retrograde eclogite-blueschist transition (FTS sequence; van der Straaten *et al.* 2012). **C)** shows a map of the La Gerbaudière quarry (Saint-Philbert-de Bouaine, Vendée) in 1999 with location of the sampling traverse (modified after Mauler *et al.* 2001 and Godard 2001).

Figure 3:

Nitrogen elemental and isotopic variations in **A**) the prograde blueschist-eclogite transition (JTS sequence, Tianshan) and **B**) the gneiss-eclogite traverse (Vendée). Additional trace element data for the JTS sequence are from Beinlich *et al.* (2010), with a precision of <5% RSD (John *et al.* 2008; van der Straaten *et al.* 2012). Uncertainties for element concentrations are smaller than the symbol size.

Figure 4:

Elemental correlations of N with other trace elements in the three profiles studied. A) JTS sequence, Tianshan, B) FTS sequence, Tianshan, C) Gneiss-eclogite traverse, Vendée.

Figure 5:

Modal content of white mica (phengite + paragonite) in rocks of the prograde blueschist-eclogite transition (JTS traverse, Tianshan; data from Beinlich *et al.* 2010) plotted versus the N concentrations.

Figure 6:

Nitrogen elemental and isotopic systematics of the analysed rocks compared to fresh MORB (Busigny *et al.* 2005), eclogites (Halama *et al.* 2010), metasedimentary rocks (Bebout and Fogel 1992; Mingram and Bräuer 2001; Busigny *et al.* 2003) and altered oceanic crust (AOC; Busigny *et*

al. 2005; Li *et al.* 2007). Colours of individual symbols are the same as in Figures 2 (JTS and FTS traverses) and 3b (Vendée traverse).

Figure 7:

Metamorphic dehydration models. **A**) Batch devolatilization (solid lines) and Rayleigh distillation (dashed lines) models of N isotopic compositions and concentrations, using the most N-rich blueschist of the JTS sequence (JTS-A) as initial composition. Isotopic fractionation by batch devolatilization is described by the equation $\delta^{15}N_f = \delta^{15}N_i - (1–F)1000 \ln \alpha$, and fractionation following Rayleigh distillation is given by the equation $\delta^{15}N_f = \delta^{15}N_i + 1000(F^{(\alpha-1)} - 1)$, where $\delta^{15}N_i$ and $\delta^{15}N_f$ and are the initial and final isotopic compositions of the rock, α is the fluid–rock fractionation factor and F is the N fraction that remains in the rock after devolatilization. Fractionation factors used in the calculations are those tabulated in Haendel *et al.* (1986) based on Hanschmann (1981) for 527 °C. Tick marks give the fraction of N remaining in the rock in 10% steps. **B**) and **C**) show calculated curves of progressive phengite dehydration by Rayleigh distillation using equations and methodology outlined in Busigny *et al.* (2003) and exchange coefficients (K_D values) based on experimental conditions of 2.0 GPa and 600 °C (Melzer and Wunder 2000), which represent a good approximation of the natural peak P-T conditions. Rayleigh distillation is modelled by fixing the initial composition and applying $K_D^{Cs\text{-}N} = 0.14$ and $K_D^{Cs\text{-}Rb} = 0.14$. Tick marks give the fraction of remaining phengite after dehydration in 10% steps.

Figure 8:

Relationships between N, $\delta^{15}N$ and Pb, CaO in the prograde blueschist-eclogite JTS sequence. The grey band indicates the average $\delta^{15}N$ value of the 9 samples from the profile, excluding the vein ($\delta^{15}N_{average} = +2.1±0.3$).

Figure 9:

Potential mixing relationships in $\delta^{15}N$–Rb/N and $\delta^{15}N$–K/N space for the Tian Shan profiles (**A**) and the Vendée profile (**B**). The field for altered oceanic crust (AOC) is based on data from the East Pacific Rise (EPR; Busigny *et al.* 2005). Compositions of (meta)sedimentary rocks are average values from five distinct locations (data from Busigny *et al.* 2003; Sadofsky and Bebout 2003, 2004; Li and Bebout 2005). Solid lines are calculated mixing curves with 10% tick marks.

Figure 10:

851 Summary figure illustrating the processes observed in the metamorphosed mafic rock sequences of
852 this study.

Fig. 1

A) Tianshan

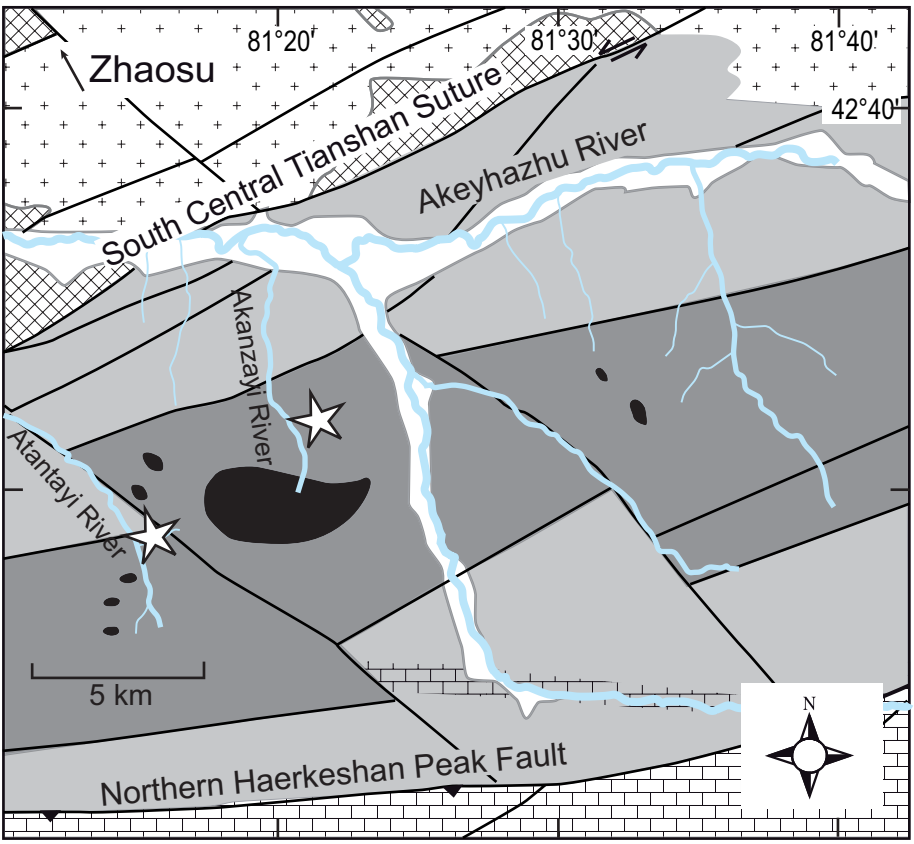

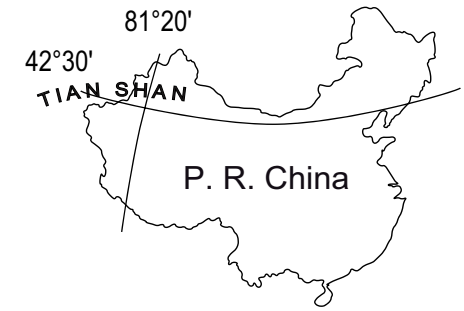

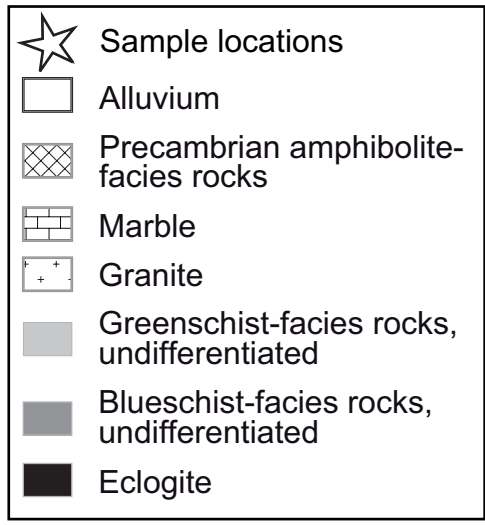

B) South Armorican Massif

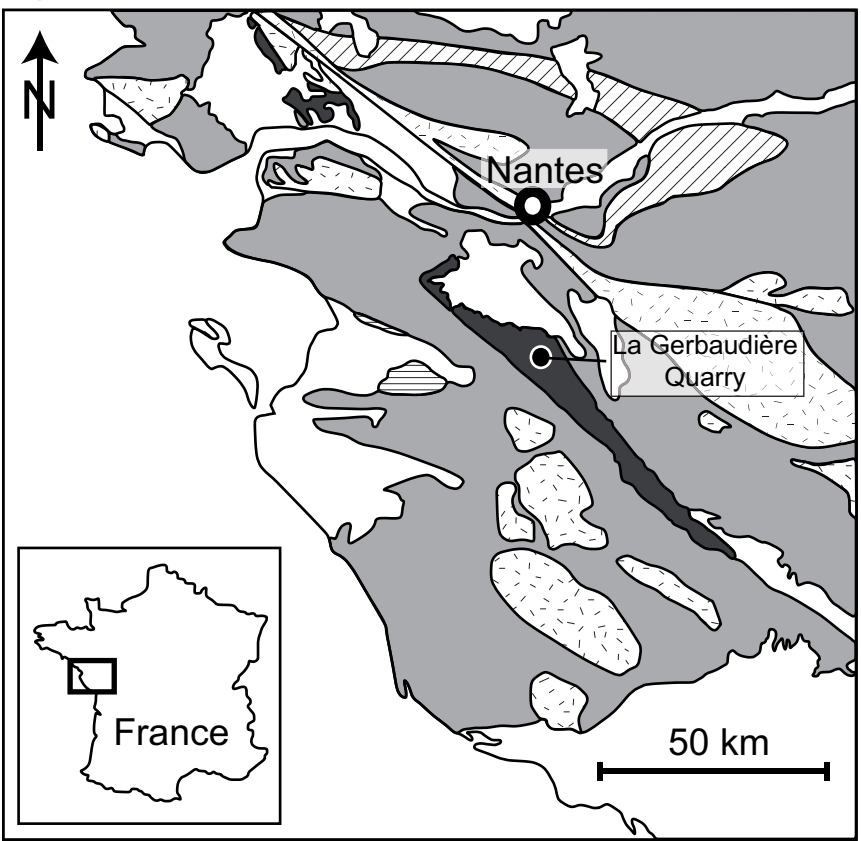

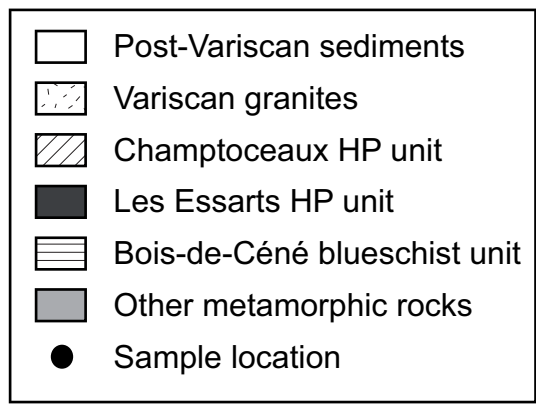

Fig. 2

A) JTS sequence

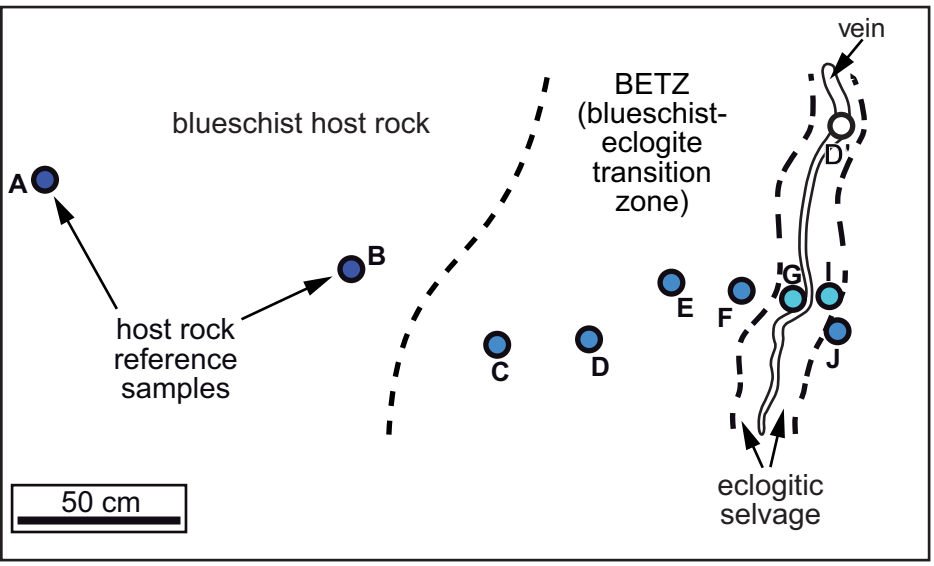

B) FTS sequence

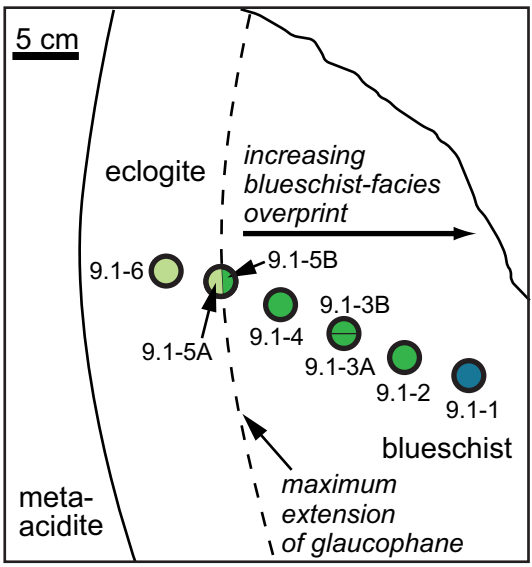

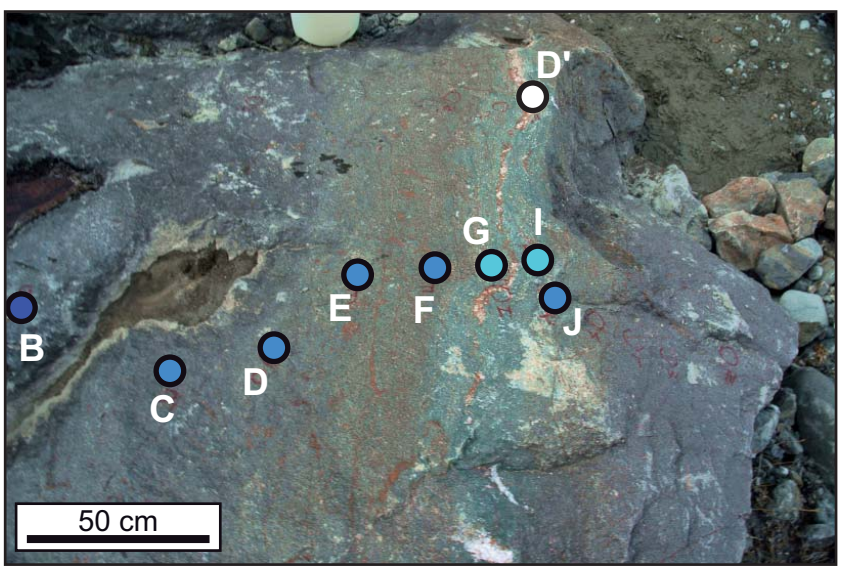

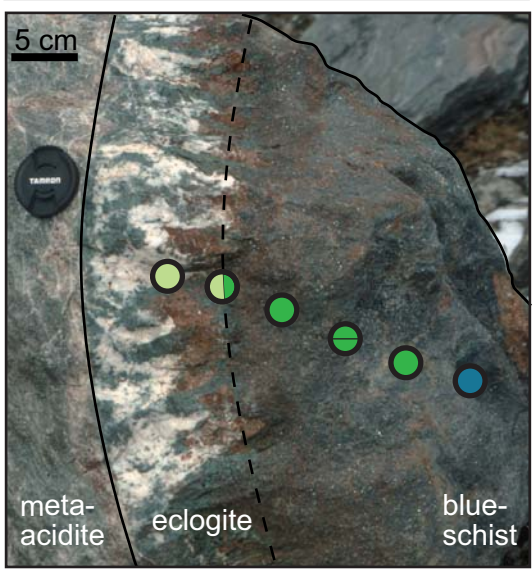

C) Vendée traverse

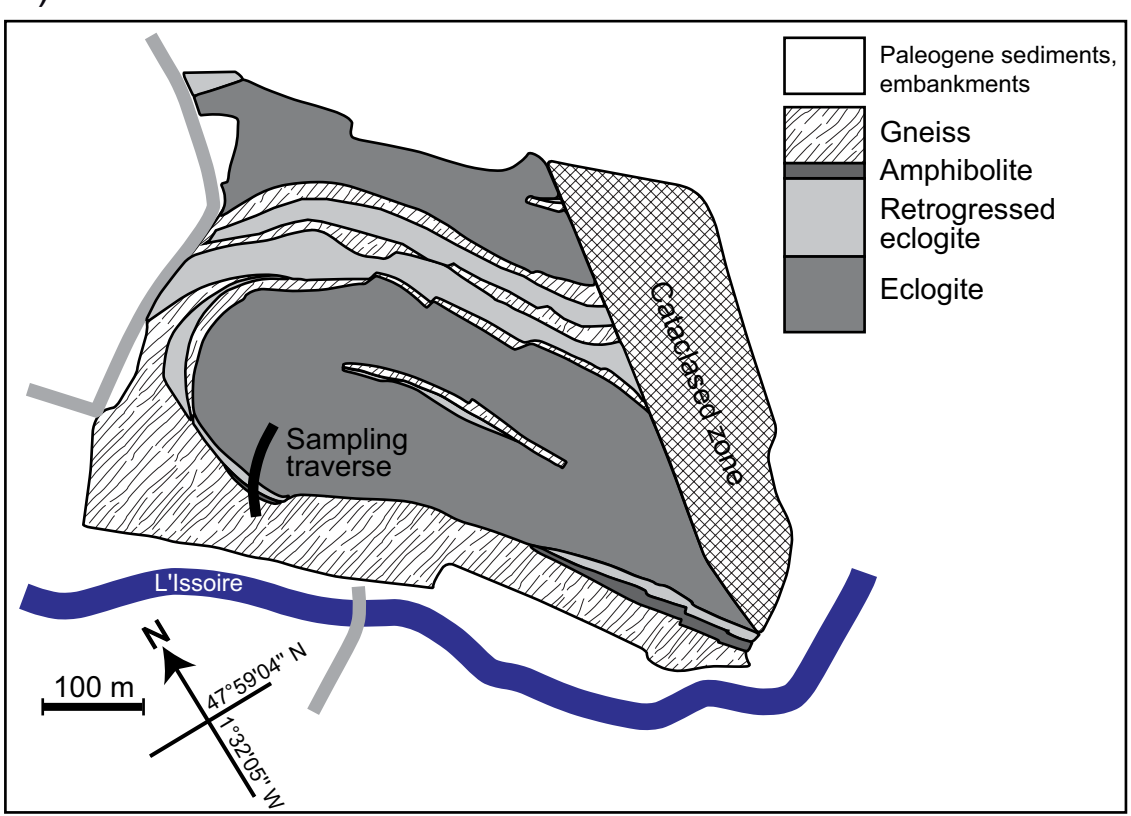

Fig. 3

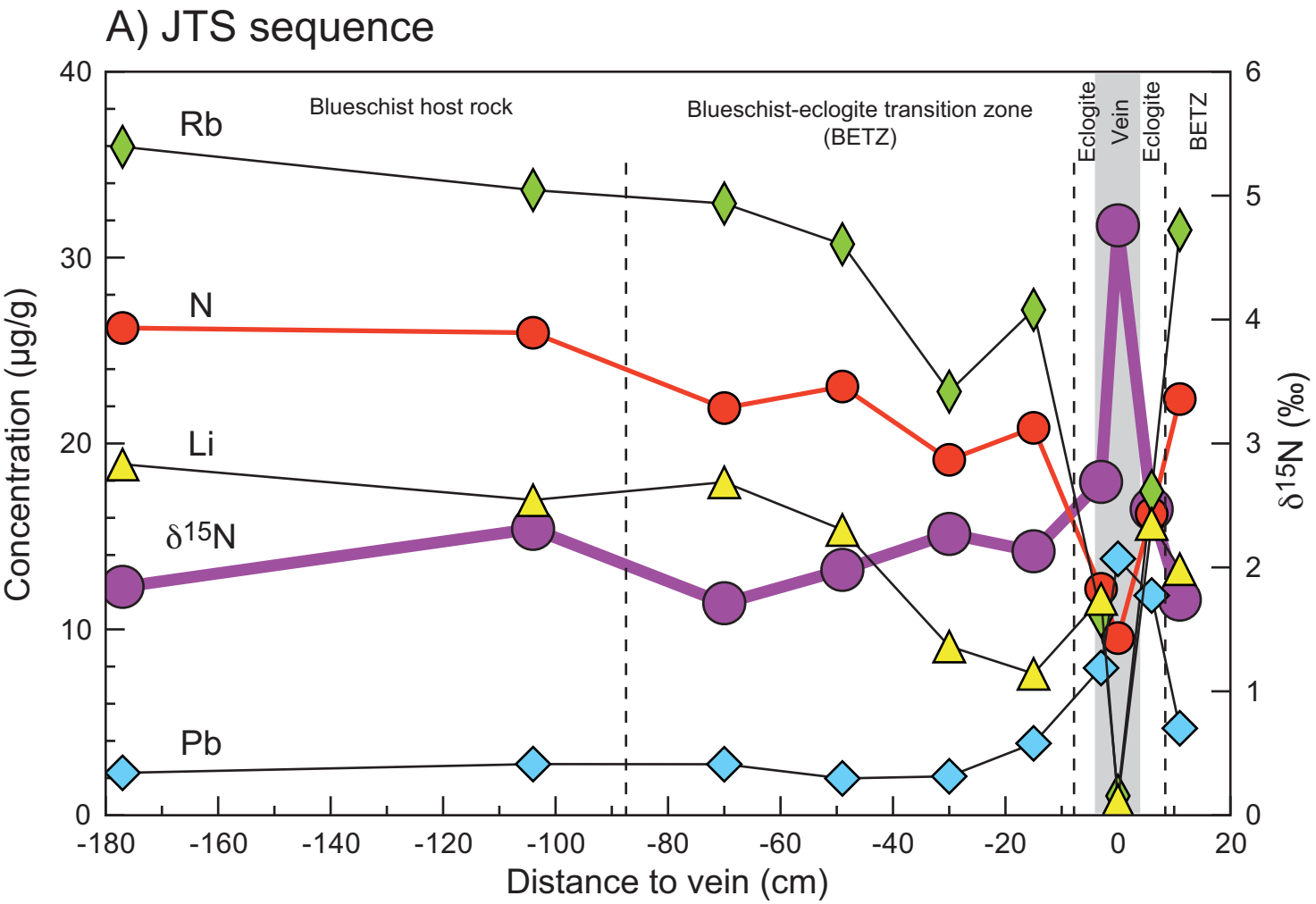
A) JTS sequence
Blueschist host rock
Blueschist-eclogite transition zone (BETZ)
Eclogite
Vein
Eclogite
BETZ
Rb
N
Li
δ15N
Pb
Concentration (µg/g)
δ15N (‰)
Distance to vein (cm)
40
30
20
10
0
6
5
4
3
2
1
0
-180
-160
-140
-120
-100
-80
-60
-40
-20
0
20

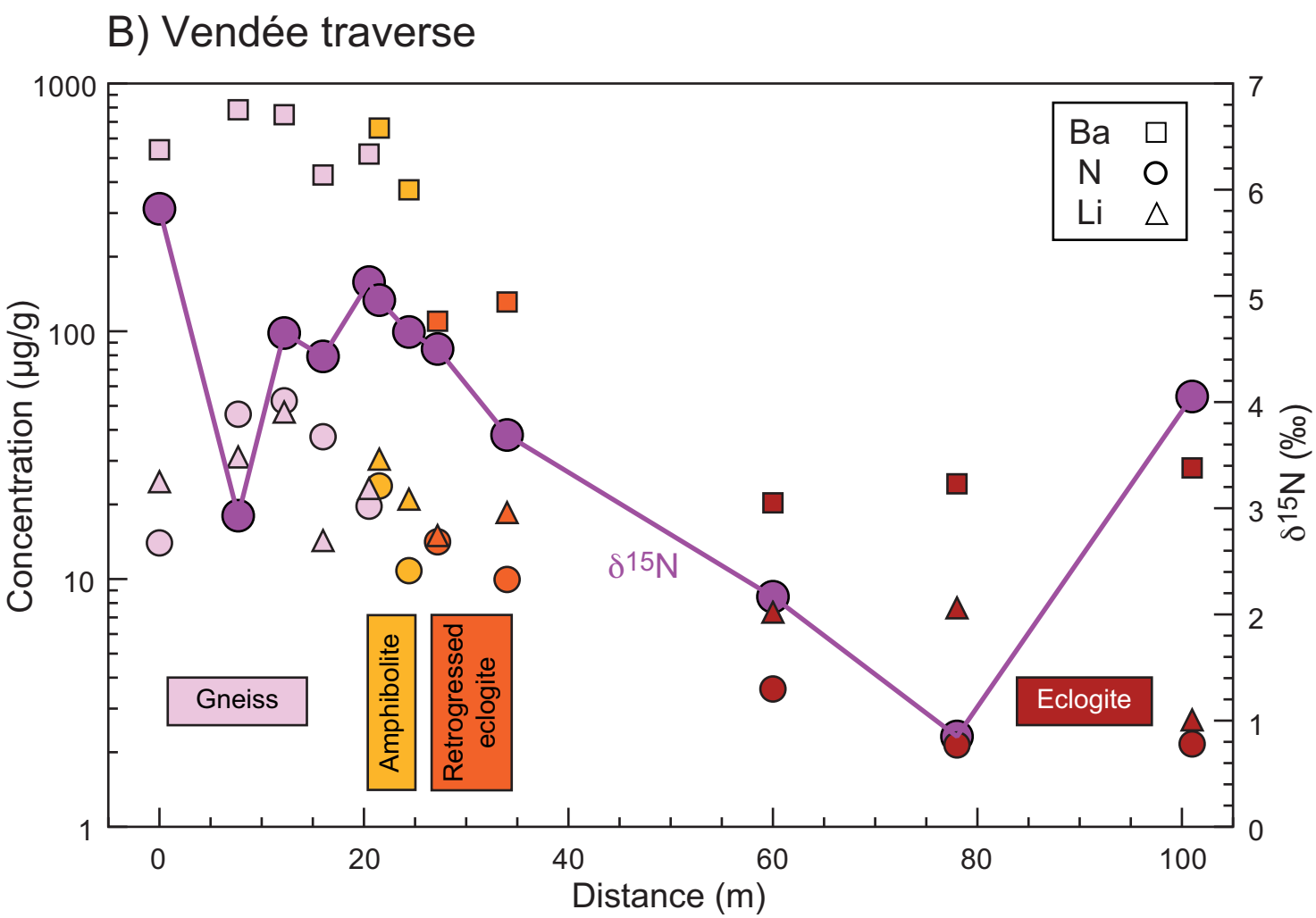
B) Vendée traverse
Ba
N
Li
δ15N
Gneiss
Amphibolite
Retrogressed eclogite
Eclogite
Concentration (µg/g)
δ15N (‰)
Distance (m)
1000
100
10
1
7
6
5
4
3
2
1
0
0
20
40
60
80
100

Fig. 4

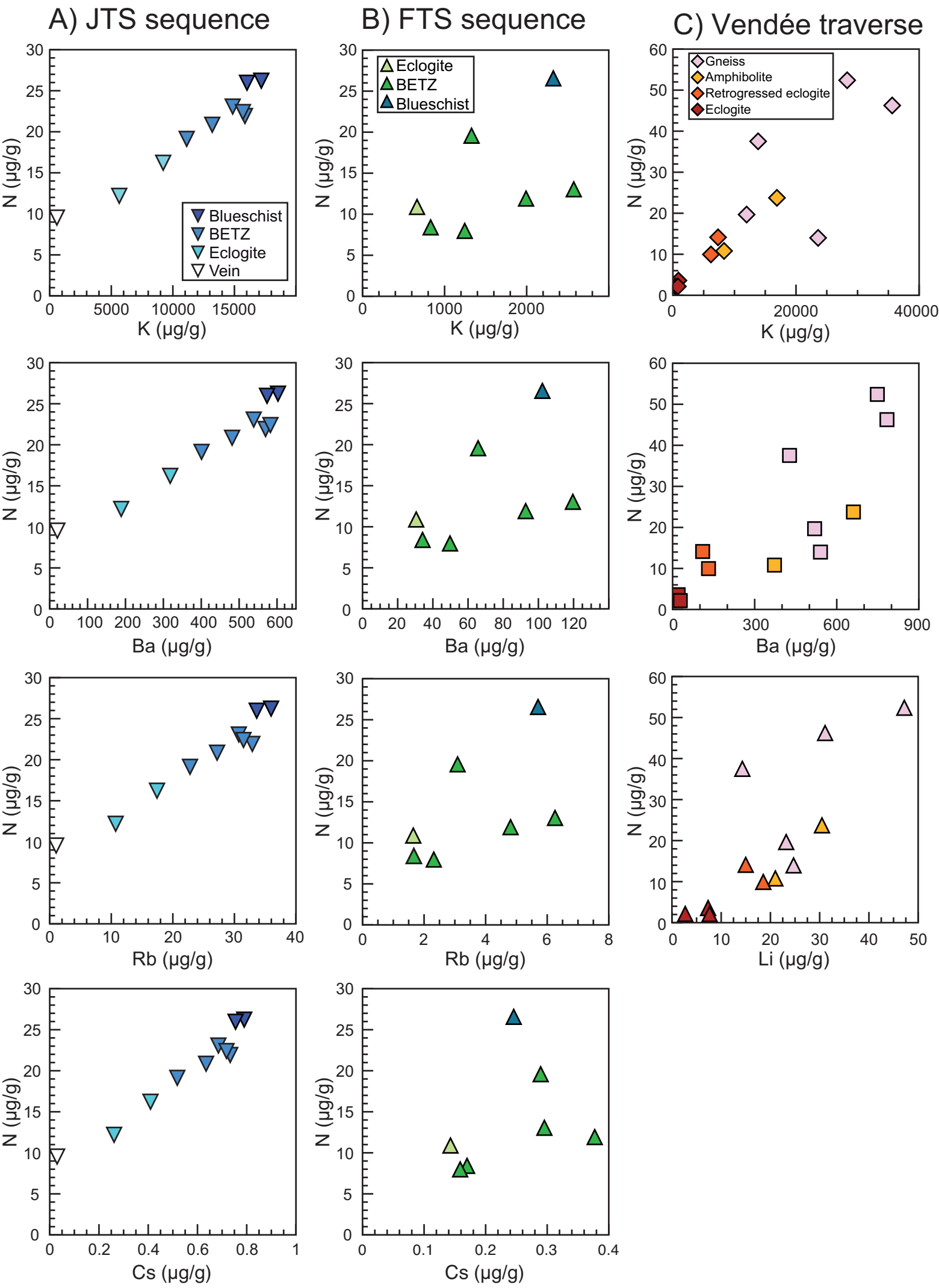
A) JTS sequence
B) FTS sequence
C) Vendée traverse
Blueschist
BETZ
Eclogite
Vein
Gneiss
Amphibolite
Retrogressed eclogite
N (µg/g)
K (µg/g)
Ba (µg/g)
Rb (µg/g)
Li (µg/g)
Cs (µg/g)

Fig. 5

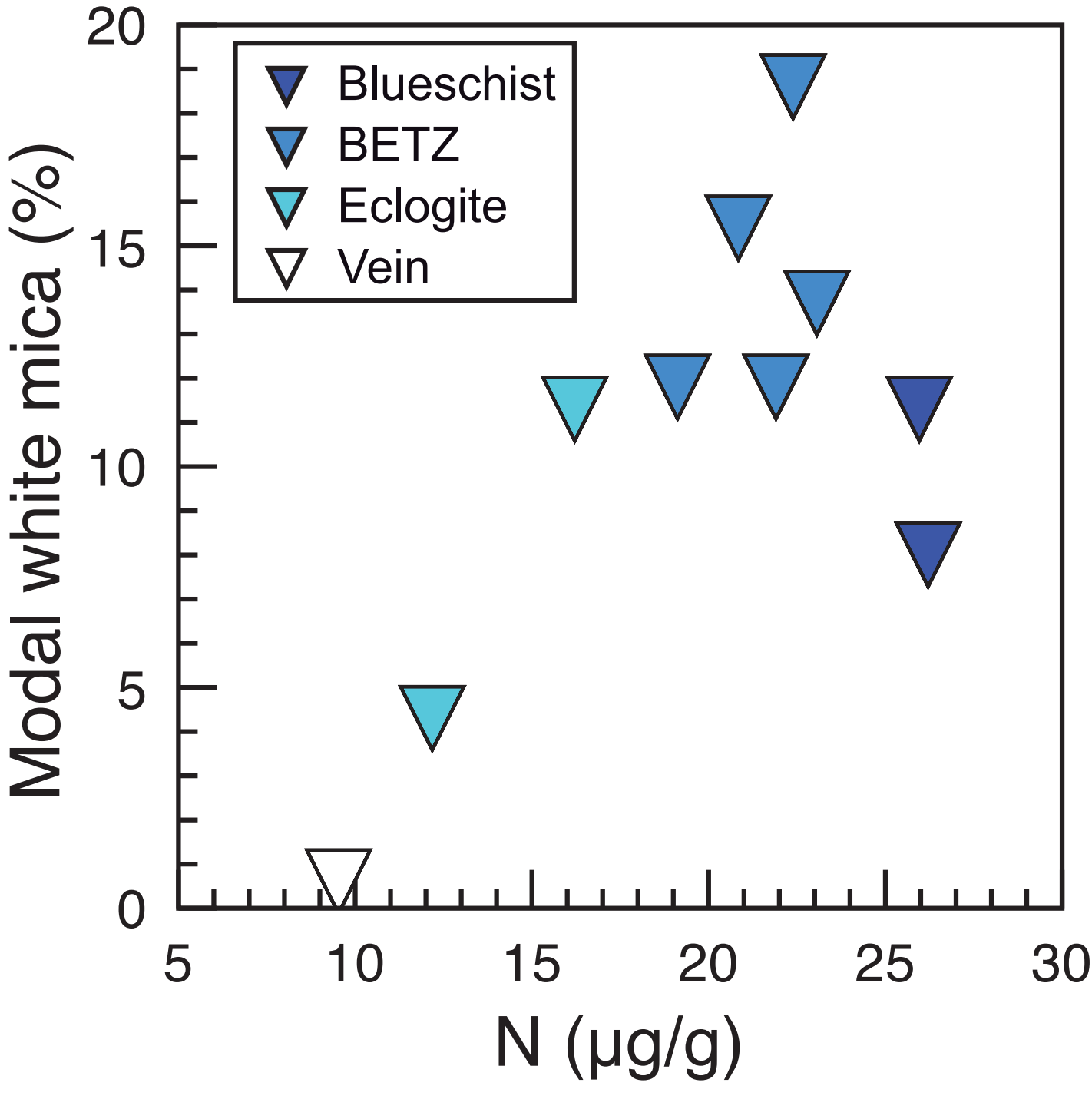
Blueschist
BETZ
Eclogite
Vein
Modal white mica (%)
N (μg/g)
0
5
10
15
20
5
10
15
20
25
30

Fig. 6

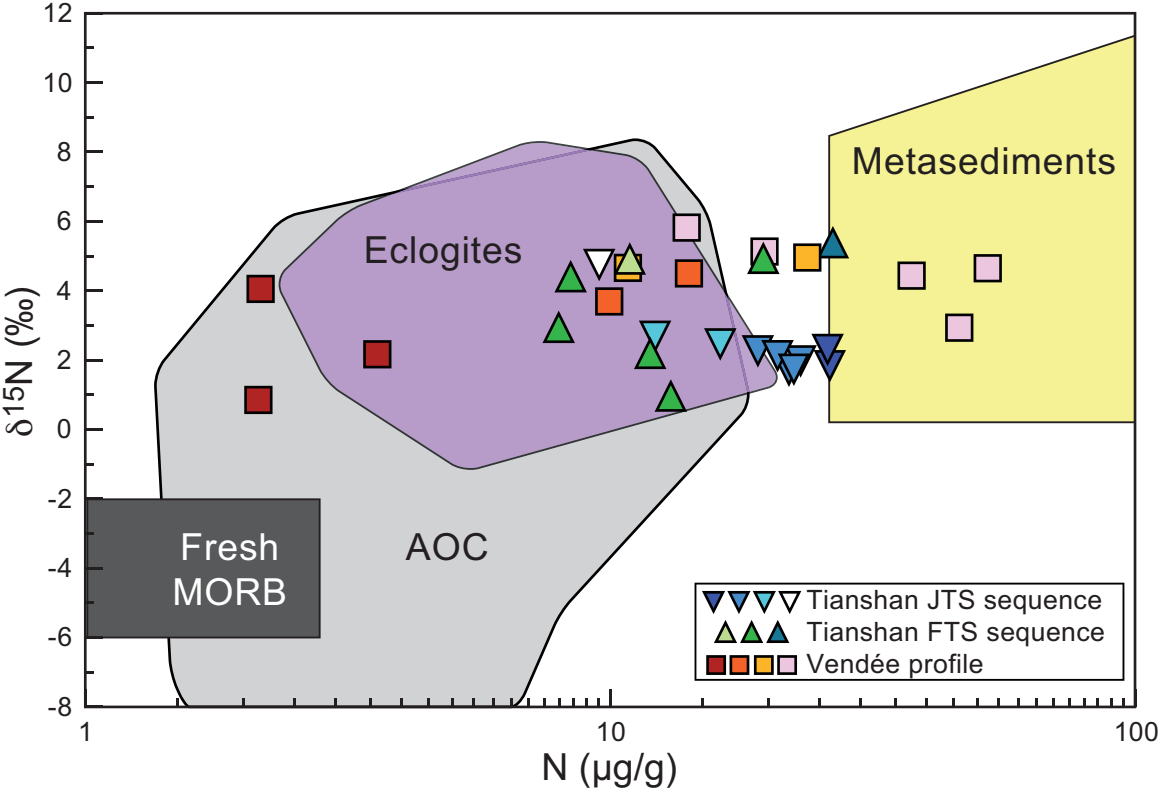
Metasediments
Eclogites
AOC
Fresh
MORB
Tianshan JTS sequence
Tianshan FTS sequence
Vendée profile
δ15N (‰)
N (μg/g)
12
10
8
6
4
2
0
-2
-4
-6
-8
1
10
100

Fig. 7

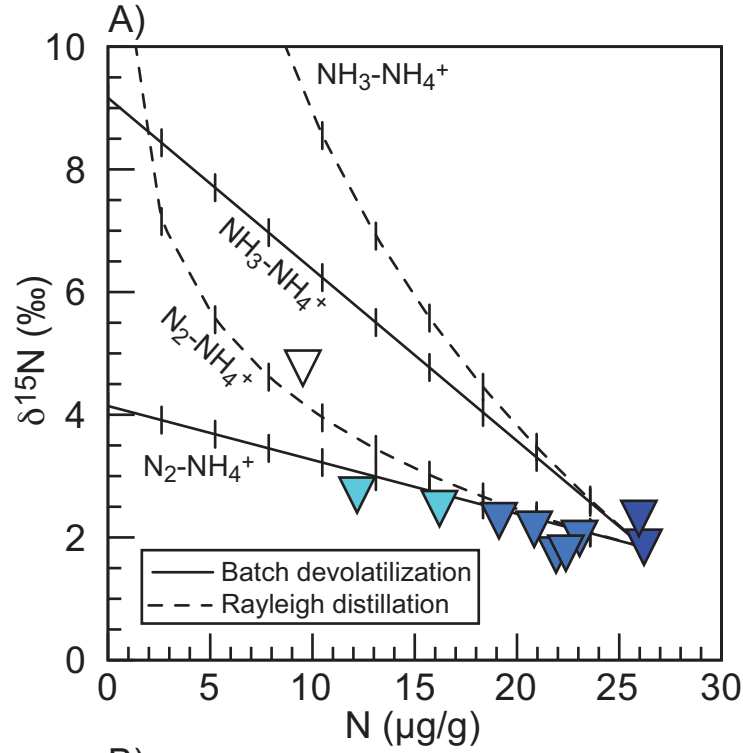
A)
NH_3-NH_4^+
NH_3-NH_4^+
N_2-NH_4^+
N_2-NH_4^+
Batch devolatilization
Rayleigh distillation
$\delta^{15}N$ (‰)
N (µg/g)

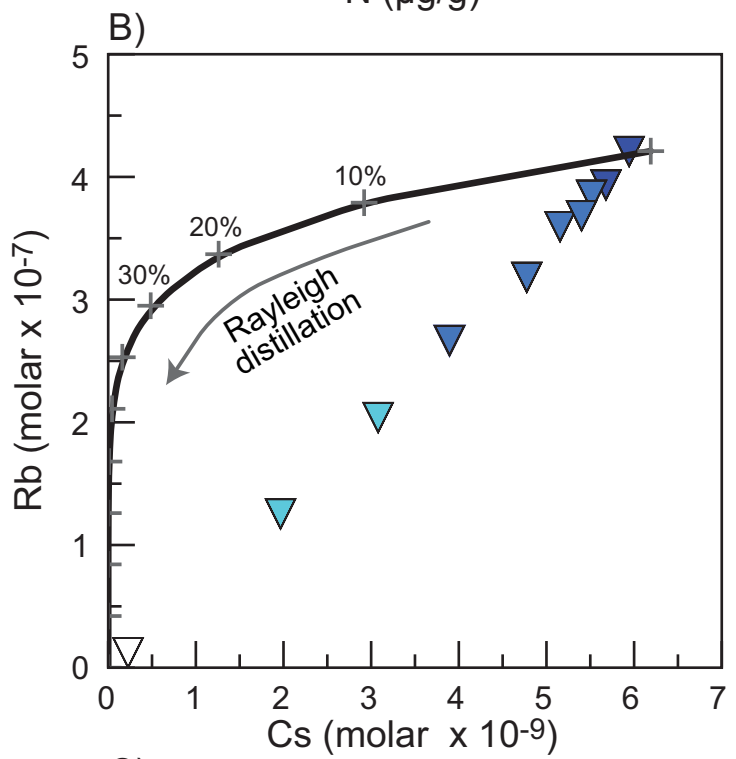
B)
10%
20%
30%
Rayleigh distillation
Rb (molar x 10^{-7})
Cs (molar x 10^{-9})

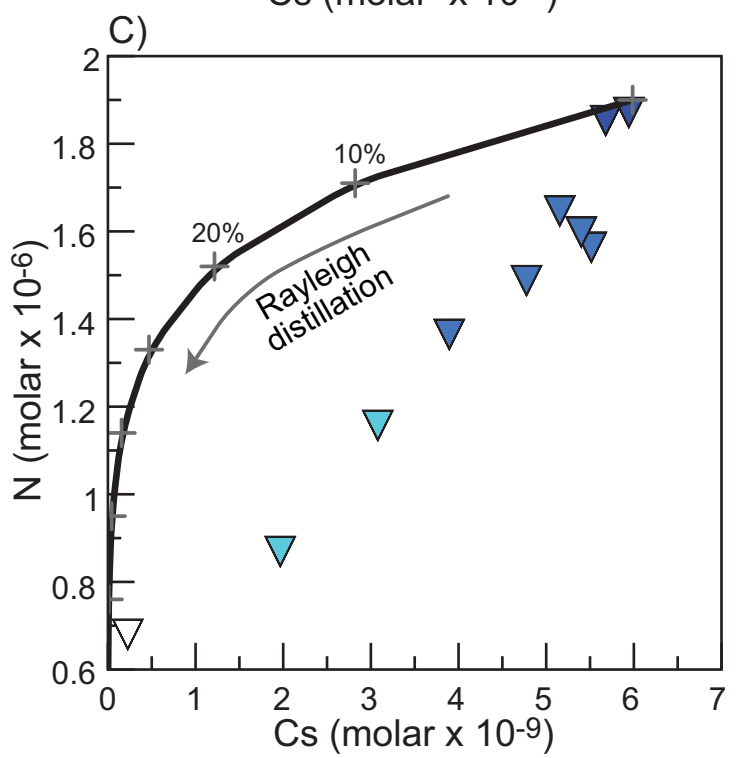
C)
10%
20%
Rayleigh distillation
N (molar x 10^{-6})
Cs (molar x 10^{-9})

Fig. 8

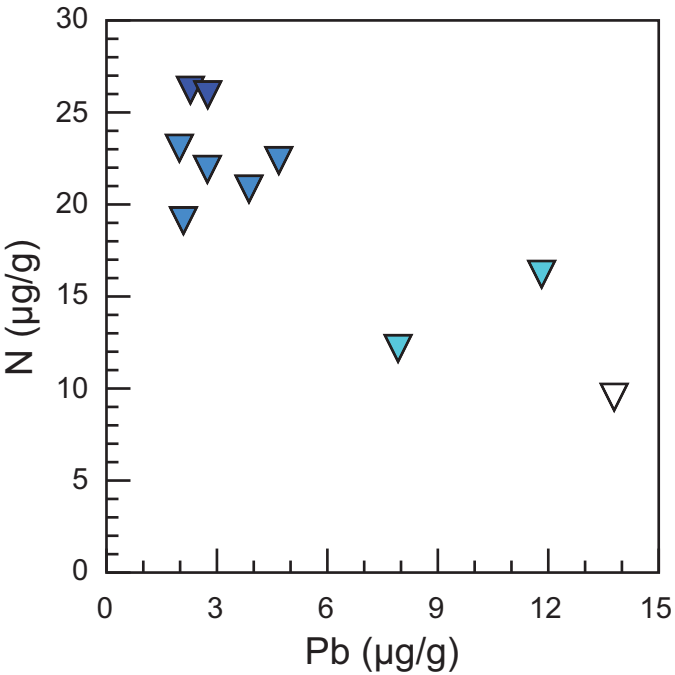

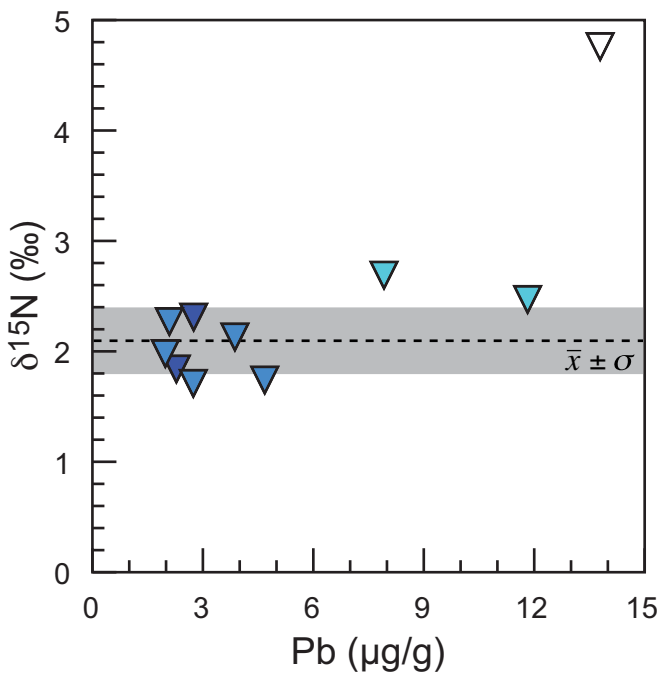

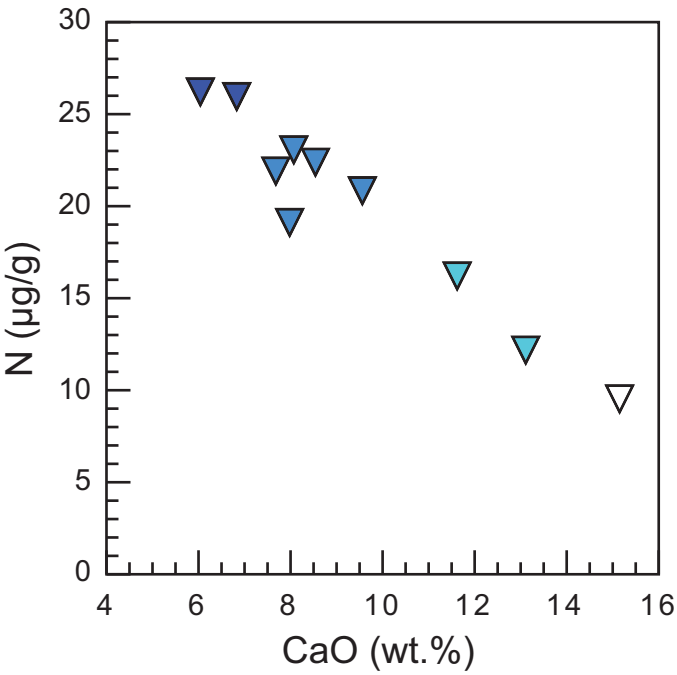

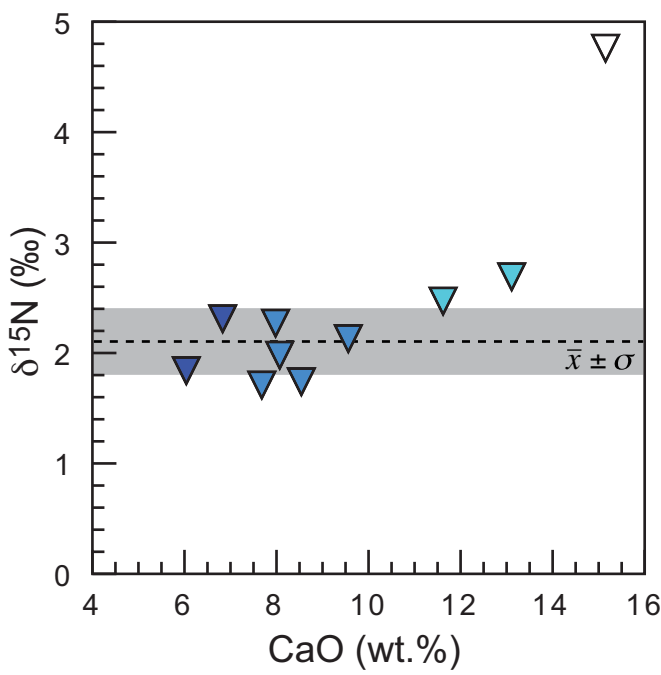

Fig. 9

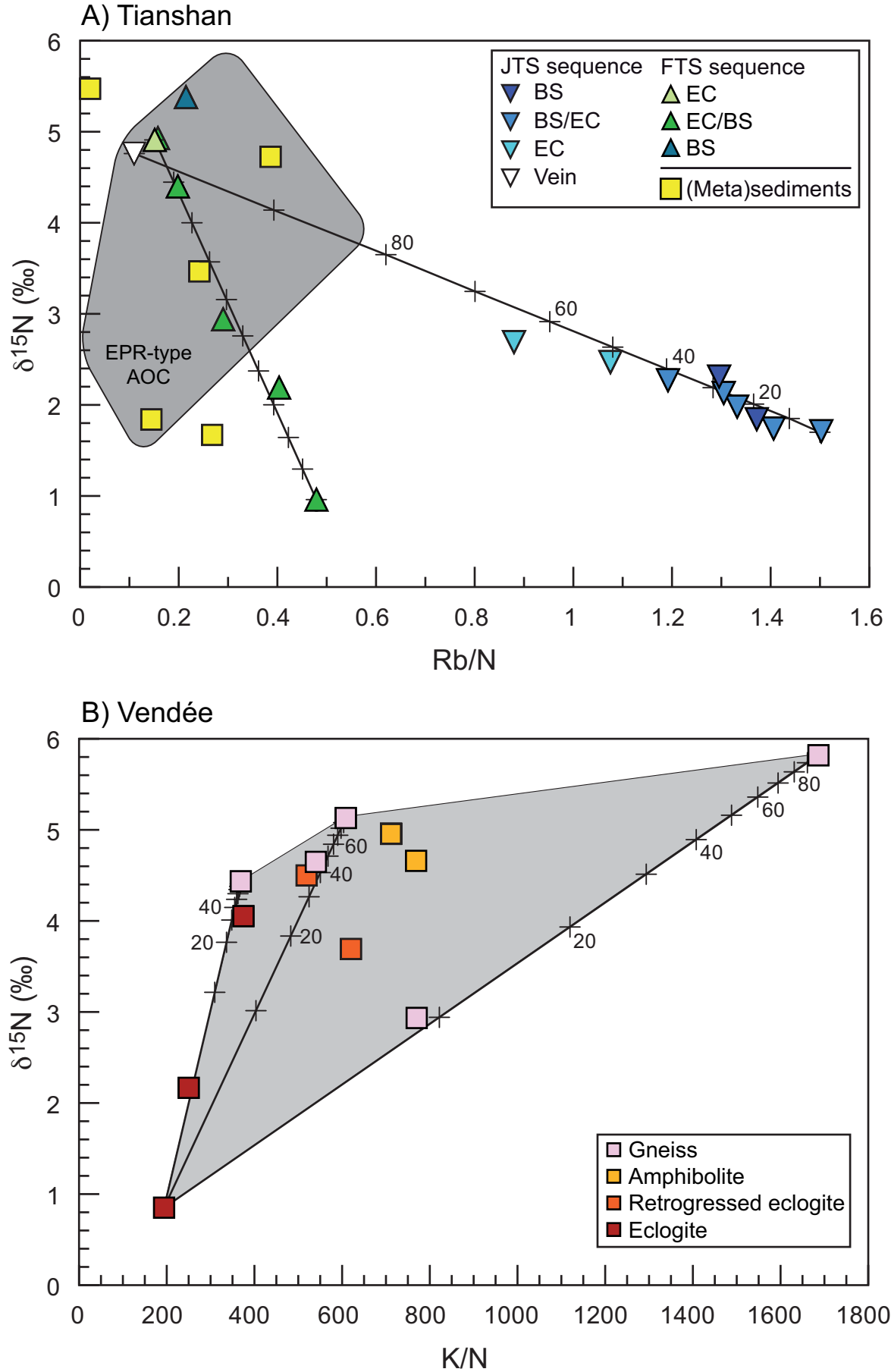
A) Tianshan
JTS sequence
BS
BS/EC
EC
Vein
FTS sequence
EC
EC/BS
BS
(Meta)sediments
EPR-type AOC
80
60
40
20
δ15N (‰)
Rb/N
0
0.2
0.4
0.6
0.8
1
1.2
1.4
1.6
0
1
2
3
4
5
6
B) Vendée
Gneiss
Amphibolite
Retrogressed eclogite
Eclogite
K/N
0
200
400
600
800
1000
1200
1400
1600
1800

Fig. 10

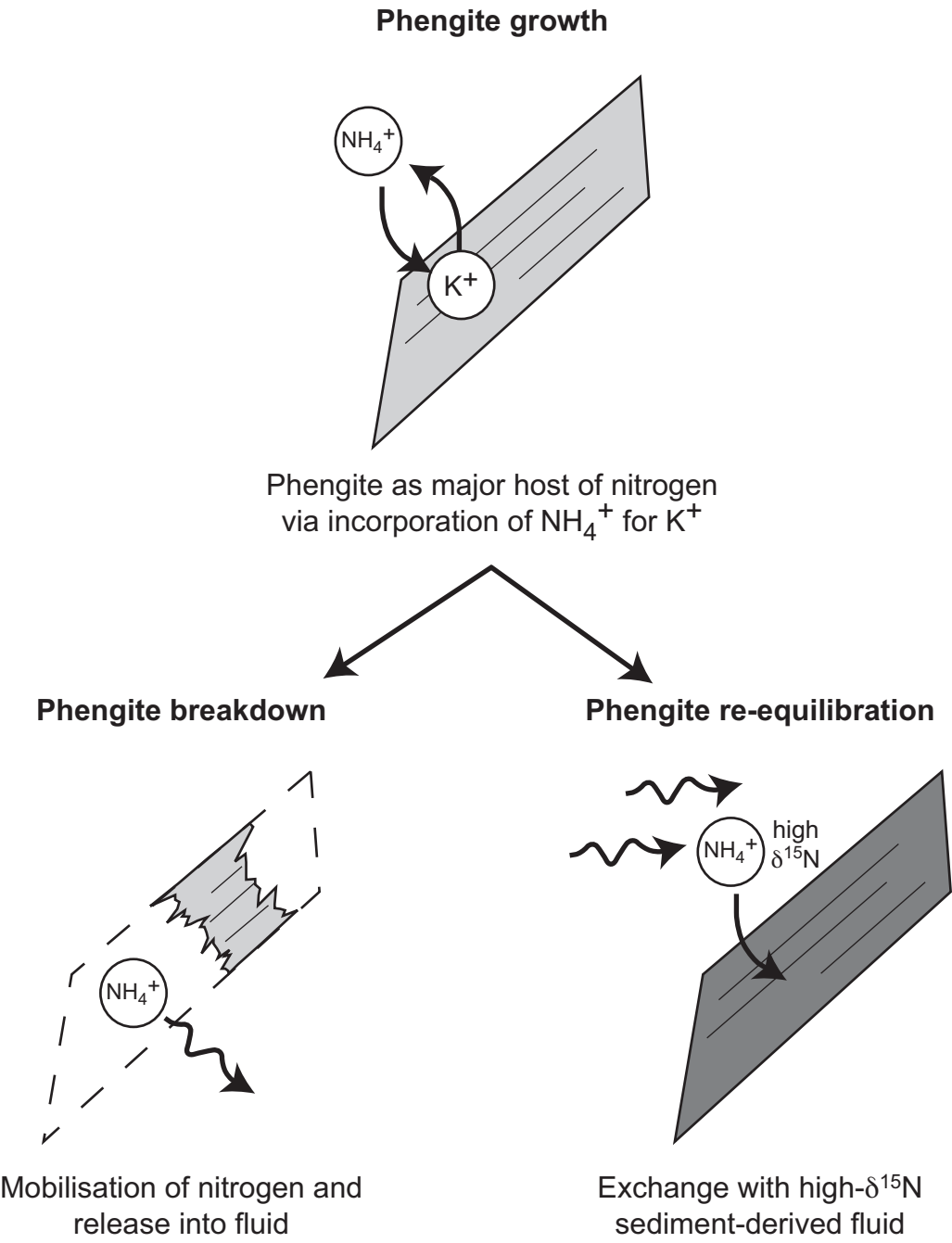
Phengite growth
NH4+
K+
Phengite as major host of nitrogen via incorporation of NH4+ for K+
Phengite breakdown
Phengite re-equilibration
NH4+
high δ15N
Mobilisation of nitrogen and release into fluid
Exchange with high-δ15N sediment-derived fluid

Table 1: Nitrogen concentration and isotope data of the three profiles investigated in this study

Sample #	**Rock-type**	**N (µg/g)**	**δ^{15}N (‰)**	**Distance (m)**
Tian Shan, prograde blueschist-eclogite transformation:				
JTS-A	blueschist	26.2	1.8	-1.77
JTS-B	blueschist	26.0	2.3	-1.04
JTS-C	bs/ec	21.9	1.7	-0.70
JTS-D	bs/ec	23.1	2.0	-0.49
JTS-E	bs/ec	19.1	2.3	-0.30
JTS-F	bs/ec	20.8	2.1	-0.15
JTS-G	eclogite	12.2	2.7	-0.03
JTS-D'	qz-carbonate vein	9.5	4.8	0
JTS-I	eclogite	16.2	2.5	0.06
JTS-J	bs/ec	22.4	1.7	0.11
Tian Shan, retrograde eclogite-blueschist transformation (FTS 9-1 sequence)				
FTS 9.1-1	blueschist	26.6	5.38	0
FTS 9.1-2	ec/bs	13.1	0.96	0.05
FTS 9.1-3 B	ec/bs	19.6	4.93	0.10
FTS 9.1-3 A	ec/bs	11.9	2.19	0.10
FTS 9.1-4	ec/bs	8.0	2.94	0.15
FTS 9.1-5 B	ec/bs	8.4	4.40	0.20
FTS 9.1-5 A	eclogite	10.9	4.91	0.20
Vendée, gneiss-to-eclogite profile				
G08-3-2	gneiss	14.0	5.8	0
G08-3-1	biotite gneiss	46.3	2.9	7.7
G08-3-3	garnet gneiss	52.4	4.6	12.2
G08-3-4	garnet gneiss	37.5	4.4	16.0
G08-3-5	gneiss	19.7	5.1	20.5
G08-3-6	garnet amphibolite	23.7	5.0	21.5
G08-3-7	garnet amphibolite	10.8	4.7	24.4
G08-3-8	retrogressed eclogite	14.1	4.5	27.2
G08-3-9	retrogressed eclogite	10.0	3.7	34
G08-3-10	eclogite	3.6	2.2	60
G08-3-11	eclogite	2.1	0.9	78
G08-3-12	eclogite	2.3	4.5	101
G08-3-12 repl.	eclogite	2.1	3.6	101
G08-3-12 avg.	eclogite	2.2	4.1	101

repl. = replicate analyses; avg. = average

Sample	JTS-A	JTS-B	JTS-C	JTS-D	JTS-E	JTS-F	JTS-J	JTS-G	JTS-I	JTS-D'	FTS 9-1.1	FTS 9-1.2	FTS 9-1.3B	FTS 9-1.3A	FTS 9-1.4	FTS 9-1.5B	FTS 9-1.5A
Traverse	JTS	JTS	JTS	JTS	JTS	JTS	JTS	JTS	JTS	JTS	FTS	FTS	FTS	FTS	FTS	FTS	FTS
Rock type	Blueschist	Blueschist	EC/BS	EC/BS	EC/BS	EC/BS	EC/BS	Eclogite	Eclogite	Vein	Blueschist	Blueschist	EC/BS	EC/BS	EC/BS	EC/BS	Eclogite
Location	Host rock	Host rock	BETZ	BETZ	BETZ	BETZ	BETZ	Selvage	Selvage	Vein	Host rock	Host rock	BETZ	BETZ	BETZ	BETZ	Selvage
Major elements (wt.%)																	
SiO_2	47.66	48.71	47.16	49.03	48.53	41.83	49.29	45.4	53.55	52.43	47.23	39.43	36.43	42.03	41.17	43.65	49.75
TiO_2	3.76	3.55	3.54	3.64	3.34	3.58	3.99	3.45	3.23	0.54	0.65	0.75	0.44	0.58	0.68	0.59	0.64
Al_2O_3	15.44	14.4	14.29	14.51	14.32	14.42	14.63	11.84	12.01	4.57	13.26	12.77	9.48	12.15	12.60	11.93	12.52
Fe_2O_3	13.52	12.99	12.39	13.29	16.22	16.62	12.35	12.93	8.76	8.86	8.23	10.84	9.27	8.65	8.81	9.30	7.94
MnO	0.19	0.2	0.16	0.2	0.29	0.28	0.14	0.19	0.05	0.12	0.11	0.35	0.23	0.17	0.22	0.24	0.20
MgO	5.53	5.31	5.87	4.47	3.64	4.72	4.13	4.72	3.9	4.22	10.29	10.30	12.28	11.23	9.69	9.27	7.59
CaO	6.04	6.83	7.68	8.07	7.98	9.56	8.54	13.11	11.62	15.15	6.66	9.86	11.90	8.67	11.12	11.72	12.28
Na_2O	3.25	3.01	3.46	3.19	1.95	1.86	2.96	3.04	3.76	0.19	5.56	4.10	4.16	4.88	4.78	5.09	5.94
K_2O	2.07	1.93	1.91	1.79	1.34	1.59	1.89	0.68	1.11	0.07	0.28	0.31	0.16	0.24	0.15	0.10	0.08
P_2O_5	0.70	0.67	0.65	0.69	0.62	0.57	0.55	0.52	0.6	2.66	0.01	0.01	0.01	0.05	0.01	0.01	0.01
CO_2	n.a.	n.a.	n.a.	n.a.	n.a.	n.a.	n.a.	n.a.	n.a.	n.a.	7.34	11.76	n.a.	11.48	10.94	8.80	3.37
$H_2O = LOI-CO_2$	n.a.	n.a.	n.a.	n.a.	n.a.	n.a.	n.a.	n.a.	n.a.	n.a.	1.68	0.47	n.a.	1.34	0.50	0.34	0.10
LOI	1.01	1.84	2.16	0.29	0.7	3.96	0.48	3.67	0.67	11.94	9.02	12.23	17.61	12.82	11.44	9.14	3.47
Total	99.17	99.44	99.27	99.17	98.93	98.99	98.95	99.55	99.26	100.75	101.30	100.95	101.97	101.47	100.67	101.04	100.42
Trace elements (µg/g)																	
Li	20.4	18.8	19.2	16.3	10.0	8.21	14.3	12.8	16.9	0.781	42.3	30.2	32.0	124	35.5	33.6	37.7
Rb	36.0	33.6	32.9	30.7	22.8	27.2	31.5	10.7	17.4	1.04	5.70	6.25	3.09	4.81	2.31	1.67	1.65
Sr	205	278	315	207	269	608	364	859	1117	2132	301	412	496	448	412	316	159
Y	49.0	47.7	36.7	47.6	78.6	55.0	49.6	37.9	37.6	27.7	13.2	38.6	15.4	13.8	22.2	16.0	18.4
Zr	382	333	340	311	303	301	342	290	279	36.3	26.7	28.6	16.2	22.7	26.7	23.5	26.2
Cs	0.790	0.755	0.733	0.685	0.518	0.635	0.718	0.261	0.409	0.03	0.25	0.30	0.29	0.38	0.16	0.17	0.14
Ba	603	574	570	539	401	481	583	189	318	20.1	102	120	65.7	92.8	49.7	34.1	30.5
Pb	2.28	2.75	2.74	1.98	2.09	3.87	4.68	7.92	11.8	13.8	3.16	3.85	4.39	4.43	3.68	2.64	1.52
Modal composition																	
Garnet	22.8	22.3	18.3	24.9	31.3	23.6	16.3	16.0	10.0	24.6							
Omphacite	16.9	17.5	29.7	34.1	30.9	26.9	39.5	50.0	50.0	5.0							
Glaucophane	36.4	28.2	23.8	6.4	2.8	1.0	0.3	0.3	–	1.5							
White mica	8.0	11.3	11.8	13.7	11.8	15.4	18.6	4.3	11.3	0.6							
Quartz	2.4	2.8	1.7	7.5	8.7	11.5	10.0	6.0	11.6	19.0							
Carbonate	0.9	5.2	4.7	0.9	2.6	12.1	0.7	7.3	1.7	38.0							
Others	12.7	12.6	10.0	12.5	11.9	9.5	14.6	15.9	15.4	11.3							

Sample	G08-3-2	G08-3-1	G08-3-3	G08-3-4	G08-3-5	G08-3-6	G08-3-7	G08-3-8	G08-3-9	G08-3-10	G08-3-11	G08-3-12
Rock type	Gneiss	Gneiss	Gneiss	Gneiss	Gneiss	Amphibolite	Amphibolite	RetEc	RetEc	Eclogite	Eclogite	Eclogite
Traverse distance (m)	0.0	7.7	12.2	16.0	20.5	21.5	24.4	27.2	34.0	60.0	78.0	101.0
Major elements (wt.%)												
SiO_2	65.16	73.59	60.19	64.84	62.96	63.17	54.21	52.53	50.62	48.02	48.86	48.16
TiO_2	0.66	0.27	1.19	0.91	0.76	0.80	0.98	0.28	0.33	1.23	1.21	1.29
Al_2O_3	15.83	13.73	15.29	14.65	15.72	15.29	16.74	21.73	18.99	14.51	14.73	15.13
Fe_2O_3	5.38	1.85	8.17	7.80	6.78	6.61	8.52	4.32	6.08	11.82	11.40	11.68
MnO	0.09	0.02	0.13	0.12	0.14	0.12	0.20	0.07	0.13	0.19	0.19	0.18
MgO	2.37	0.56	3.66	2.23	2.78	2.67	5.63	5.04	7.58	7.98	8.02	8.06
CaO	2.22	1.17	3.04	2.70	3.03	2.28	7.42	10.93	10.87	12.40	11.28	12.17
Na_2O	3.15	3.02	1.89	2.84	3.35	3.67	2.90	2.70	2.82	2.18	3.20	2.41
K_2O	2.84	4.29	3.41	1.67	1.44	2.04	1.00	0.88	0.74	0.11	0.05	0.10
P_2O_5	0.20	0.10	0.19	0.11	0.16	0.10	0.13	0.02	0.02	0.10	0.10	0.10
LOI	1.45	0.82	2.23	1.41	1.96	2.08	1.91	1.56	1.78	0.72	0.41	0.52
Total	99.35	99.41	99.38	99.28	99.09	98.83	99.63	100.06	99.95	99.25	99.45	99.79
Trace elements (µg/g)												
Li	24.7	31.1	47.2	14.3	23.2	30.5	21.0	15.0	18.5	7.35	7.65	2.70
Cr	20.3	b.d.l.	72.2	35.1	30.3	42.9	169	52.7	147	258	202	215
Ni	b.d.l.	b.d.l.	5.0	10.2	3.1	2.8	28.7	b.d.l.	1.8	59.5	31.5	38.3
Sr	240	142	245	258	357	355	281	813	406	147	126	125
Zr	190	149	241	356	244	297	188	15.6	14.5	81.0	80.9	89.1
Ba	540	784	748	427	519	661	372	110	131	20.3	24.2	28.1

RetEc = Retrogressed eclogite
b.d.l. = below detection limit